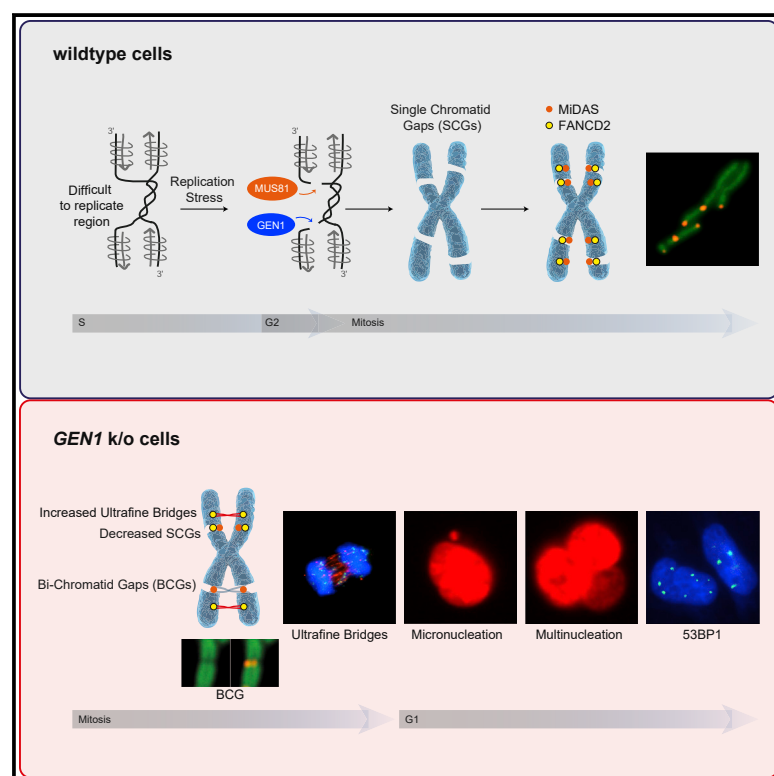# GEN1 promotes common fragile site expression

Graphical abstract

Authors

Anaid Benitez, Marie Sebald,
Radhakrishnan Kanagaraj,
Monica C. Rodrigo-Brenni,
Ying Wai Chan, Chih-Chao Liang,
Stephen C. West

Correspondence

stephen.west@crick.ac.uk

In brief

Following replication stress, common fragile sites (CFSs) are cytologically visualized as DNA gaps and breaks. This CFS "expression" is dependent on the structure-selective nucleases MUS81-EME1 and XPF-ERCC1. Benitez et al. find that GEN1 nuclease also promotes CFS expression, indicating that it resolves replication and recombination intermediates to facilitate chromosome segregation.

Highlights

- GEN1 nuclease promotes common fragile site expression following replication stress

- Loss of GEN1 leads to reduced mitotic DNA replication (MiDAS) and anaphase bridges

- Anaphase bridge formation leads to DNA damage in the next cell cycle

- GEN1 plays a dual cellular role, resolving replication and recombination intermediates

Article

GEN1 promotes common fragile site expression

Anaid Benitez,[1] Marie Sebald,[1] Radhakrishnan Kanagaraj,[1,2] Monica C. Rodrigo-Brenni,[1,3] Ying Wai Chan,[1,4] Chih-Chao Liang,[1] and Stephen C. West[1,5,*]

[1]The Francis Crick Institute, DNA Recombination and Repair Laboratory, 1 Midland Road, London NW1 1AT, UK
[2]Present address: School of Life Sciences, University of Westminster, London W1W 6UW, UK, and School of Life Sciences, University of Bedfordshire, Park Square, Luton LU1 3JU, UK
[3]Present address: AstraZeneca, Cambridge CB2 0AA, UK
[4]Present address: School of Biological Sciences, University of Hong Kong, Hong Kong
[5]Lead contact
*Correspondence: stephen.west@crick.ac.uk
https://doi.org/10.1016/j.celrep.2023.112062

SUMMARY

Our genomes harbor conserved DNA sequences, known as common fragile sites (CFSs), that are difficult to replicate and correspond to regions of genome instability. Following replication stress, CFS loci give rise to breaks or gaps (termed CFS expression) where under-replicated DNA subsequently undergoes mitotic DNA synthesis (MiDAS). We show that loss of the structure-selective endonuclease GEN1 reduces CFS expression, leading to defects in MiDAS, ultrafine anaphase bridge formation, and DNA damage in the ensuing cell cycle due to aberrant chromosome segregation. GEN1 knockout cells also exhibit an elevated frequency of bichromatid constrictions consistent with the presence of unresolved regions of under-replicated DNA. Previously, the role of GEN1 was thought to be restricted to the nucleolytic resolution of recombination intermediates. However, its ability to cleave under-replicated DNA at CFS loci indicates that GEN1 plays a dual role resolving both DNA replication and recombination intermediates before chromosome segregation.

INTRODUCTION

Faithful replication of the genome is fundamental for cell viability and disease avoidance. Replication initiates at specific regions, defined as origins, and proceeds bidirectionally until a converging replication fork is encountered. However, some regions of the genome, known as common fragile sites (CFSs), are intrinsically difficult to replicate and lead to the formation of single chromatid gaps (SCGs) or breaks and bichromatid gaps (BCGs) or constrictions upon replication stress. The formation of gaps, which are visible on condensed metaphase chromosomes, is defined as CFS "expression," and it is particularly evident after replication stress.[1]

Under-replication of the genomic loci at CFSs impacts mitotic chromosome segregation, resulting in DNA damage in the resulting G1 cells, and it is linked to chromosome instability and disease.[2,3] Indeed, CFSs represent hotspots for cancer-specific chromosomal aberrations such as deletions, amplifications, translocations, and rearrangements.

CFS instability is cell type specific and observed in cultured cells and mouse models after replication stress induced by partial DNA polymerase inhibition or nucleotide pool imbalance.[4,5] Instability also arises from oncogene activation, which in turn induces replication stress, but the fragility landscape only partially overlaps with DNA polymerase inhibition-induced fragility.[6] These observations imply that there are additional levels of

complexity underlying the recurrent fragilities seen in cancer cells.

Over 100 CFSs have been identified and are detailed in the human fragile site database (humCFS).[7] They are often found within large and actively transcribed genes where transcription-replication collisions occur.[8–12] CFS instability is also associated with a paucity of replication origins,[13] delayed replication timing,[5,14–16] 3D genome architecture,[16] histone hypoacetylation,[17] faulty condensin loading,[18] and the presence of difficult-to-replicate AT-rich sequences that form secondary structures.[19–22]

Treatment of cells with low-dose aphidicolin (APH), an inhibitor of B-family DNA polymerases,[23] leads to genome-wide delays in DNA replication, culminating in the formation of under-replicated DNA intermediates in late S and G2 phase, particularly at already late-replicating CFS loci.[5,24] A useful marker for these loci is FANCD2, which is defective in individuals with Fanconi anemia subgroup D2.[25,26] FANCD2 and FANCI interact to form a complex that is monoubiquitylated upon fork stalling and can be visualized by immunofluorescence as twin FANCD2 foci in late S, G2, and M phase.[27–29]

Following mild replication stress and gradual fork slowing, repetitive DNA sequences within CFSs may fold to form stable secondary structures that further impede fork progression. These secondary structures might be important for fragility, as they serve as targets for the structure-selective endonucleases MUS81-EME1 and XPF-ERCC1.[30,31] Both nucleases associate

with the SLX4 scaffold, and with SLX1, to form the SMX trinuclease complex comprising SLX1-SLX4, MUS81-EME1, and XPF-ERCC1.[32,33] SMX complex plays an important cellular role in processing branched DNA structures including under-replicated DNA at stalled/collapsed replication forks, late replication intermediates, and recombination intermediates. Following endonuclease cleavage, the under-replicated regions manifest as DAPI-negative SCGs on metaphase chromosomes.[30,31,34]

To ensure that under-replicated regions of the genome are successfully duplicated, a repair mechanism known as mitotic DNA synthesis (MiDAS) is activated.[29] MiDAS is dependent upon the activity of MUS81-EME1 and driven by Pol δ[29], although translesion polymerases such as Pol ζ (REV3) and η (POLH) have also been implicated.[35–37] MiDAS is thought to mediate repair via break-induced replication (BIR), a process that can induce genome duplications.[38]

Although the MUS81-EME1 and XPF-ERCC1 endonucleases both cleave replication intermediates,[30,31] their combined depletion fails to completely suppress CFS expression, indicating the involvement of other nuclease(s). The role of endonucleases in CFS expression has been investigated in yeast. Using a model system in which FLEX1, an AT-rich region derived from the fragile site locus FRA16D, was inserted into an artificial chromosome, it was shown that loss of *mus81* or *slx4* decreased fragility.[39] In contrast, loss of *yen1*, which encodes the yeast ortholog of human GEN1,[40] led to increased fragility, indicating a protective role against FLEX1-induced fragility.[39] One possibility is that Yen1 might act upon a different structure than Mus81-Mms4, such as a DNA intermediate containing two replication forks that had not merged. We therefore investigated a potential role for human GEN1 in CFS processing.

Like SMX, GEN1 is a structure-selective endonuclease that cleaves recombination intermediates (Holliday junctions) and replication forks *in vitro*.[33,40–43] However, in contrast to MUS81-EME1 and SMX, GEN1 has a nuclear export sequence and primarily localizes to the cytoplasm.[44] One possibility is that GEN1 might cleave unresolved replication intermediates during mitosis when under-replicated DNA is exposed to cytosolic proteins upon nuclear envelope breakdown.[44] In this study, we found that GEN1 promotes replication-stress-induced CFS expression, and that GEN1 loss leads to an elevated frequency of bichromatid constrictions consistent with the persistence of unresolved regions of under-replicated DNA. We also found that MiDAS occurs after the nucleolytic activity of GEN1 and involves Pol δ-dependent DNA replication. We describe the consequences of GEN1 loss after replication stress and observe ultrafine anaphase bridge formation and DNA damage due to defects in chromosome segregation.

RESULTS

GEN1 promotes CFS expression

To determine whether GEN1 promotes CFS expression, we generated pool and single cell *GEN1* knockouts (KOs) in HEK293 and U2OS cell lines, respectively, using CRISPR-Cas9. The *GEN1* KOs were verified by immunoblotting and sequencing of the U2OS clone (Figures S1A and S1B). Genome-wide analysis of replication dynamics in human cells in-

dicates that >300 genomic regions exhibit delayed replication upon APH treatment.[5,16] Consistent with these observations, treatment of HEK293, U2OS wild-type (WT), and the *GEN1* KO cells with APH for 24 h led to an increased number of cells in S and G2/M phases of the cell cycle (Figures S1C–S1E). These effects were partly reversible upon 24 h release from APH, resulting in a mild recovery of the original cell cycle dynamics (Figure S1F). Longer treatment with APH (48 h) resulted in a similar change to the percentage of cells in S and G2/M (Figure S1G).

GEN1 KOs were next analyzed for the appearance of cytogenetic aberrations in response to replication stress. For comparison, we used isogenic cell lines knocked out for MUS81 or both GEN1 and MUS81. We observed reduced single chromatid gap formation in HEK293 *GEN1* KO cells compared with WT HEK293 cells after APH treatment (Figures 1A and 1B). Similar results were obtained with U2OS *GEN1* KO cells (Figure S1H). Similarly, when GEN1 was depleted from U2OS cells using siRNA, we again observed reduced SCG formation (Figures S1I and S1J).

To compare the relative contribution of GEN1 and MUS81-EME1 to CFS expression, we quantified APH-induced SCGs in the HEK293 *GEN1* KO pool, the *MUS81* KO, and the double *GEN1 MUS81* KO. Loss of GEN1 reduced SCGs to a similar extent as that observed in the *MUS81* KO (Figures 1A and 1B). Because attempts at making double *GEN1 MUS81* KOs were unsuccessful, we created fresh pool KOs for these short-term assays. The *GEN1 MUS81* double KOs did not exhibit a further reduction in SCG formation compared with *GEN1* KO alone. Similar results were observed when MUS81 was siRNA depleted from U2OS *GEN1* KO cells (Figures S1B and S1H) or when both nucleases were siRNA depleted (Figures S1I and S1J). These results show that GEN1 and MUS81-EME1 can both promote the appearance of cytogenic SCGs upon replication stress in HEK293 and U2OS cells.

GEN1 associates with chromatin

CFS expression by MUS81-EME1 and their subsequent repair occurs prior to prometaphase.[29] We therefore determined the stage at which GEN1 nuclease might act upon secondary structures arising within CFSs. Previous immunofluorescence analyses and cellular fractionation studies showed that over-expressed GFP-tagged GEN1 was approximately 80% cytoplasmic and 20% nuclear.[44] Sub-cellular fractionation of unchallenged and APH-treated HEK293 cells revealed that endogenous GEN1 co-extracted with α-tubulin, indicating it was primarily cytoplasmic, but there was a significant portion of the protein in the nucleus (approximately 25%), of which a sub-fraction was bound to chromatin, as determined by western blotting (Figure 2A).

We next analyzed the association of GEN1 with chromatin by iPOND (isolation of proteins on nascent DNA).[45] This assay examines the interaction of proteins with ongoing replication forks that have incorporated the thymidine analog 5-ethynyl-2′-deoxyuridine (EdU) into newly synthesized DNA during a short 10-min incubation (Figure S2A). The iPOND assay confirmed the binding of GEN1 to chromatin (Figures 2B and S2B). PCNA (proliferating cell nuclear antigen), FANCD2, and MUS81, which are known to associate with the replication fork upon replication stress, were used as controls. To distinguish between proteins associated with the fork and chromatin in general, we used thymidine-containing media to chase the EdU-labeled region away from the
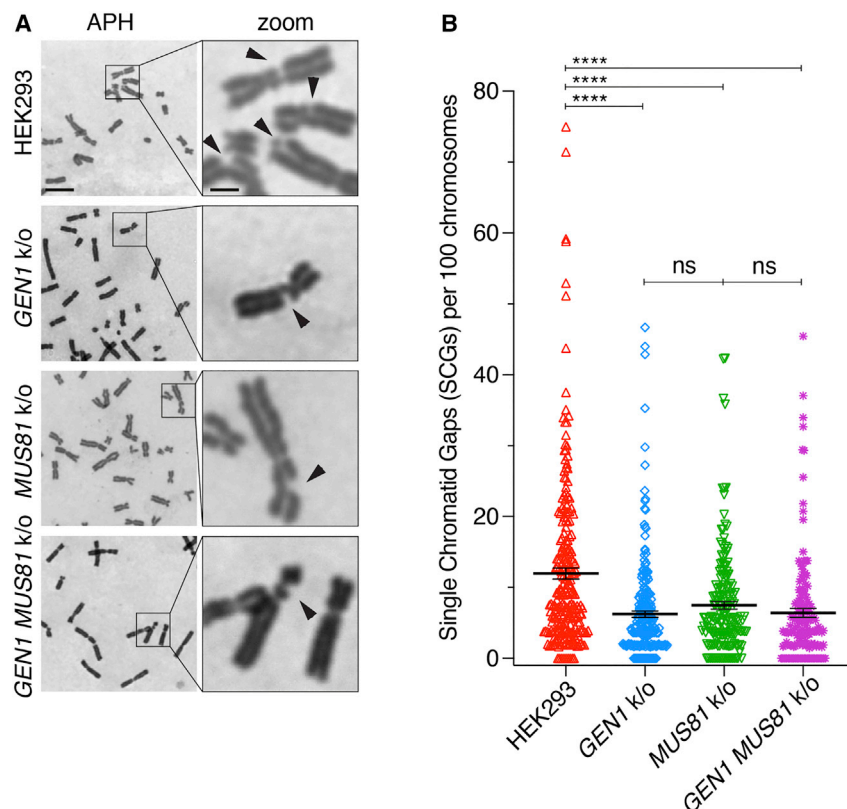
Figure 1. *GEN1* loss causes decreased CFS expression following replication stress

(A) Representative images of Giemsa-stained metaphase spreads of HEK293, *GEN1* KO, *MUS81* KO, and *GEN1 MUS81* KO cells after treatment with aphidicolin (APH, 0.4 μM) for 24 h. Arrows indicate single chromatid gaps (SCGs). Scale bars represent 5 μm and 1 μm (zoom).

(B) Quantification of SCGs per 100 chromosomes, as in (A). 240 HEK293, 240 *GEN1* KO, 180 *MUS81* KO, and 150 *GEN1 MUS81* KO cells were scored. Data are represented as mean ± SEM; n = 3. See also Figure S1.

which has both 5′ flap/fork (SLX1-SLX4) and 3′ flap/fork (MUS81-EME1 and XPF-ERCC1) activities, could incise RPA-coated replication structures. We found that RPA inhibited SMX-mediated cleavage of the 5′ and 3′ flap/fork structures to a greater extent than observed with GEN1 (Figures 2E and 2F). These results indicate that GEN1 is effective at cleaving 5′ flap/fork structures that may arise at replication forks following under-replication.

GEN1 loss leads to fewer stress-induced SCGs and reduced MiDAS

Following replication stress, FANCD2 forms twin foci during late S/G2, which can be visualized on SCGs and BCGs, and it facilitates mitotic replication at CFSs.[28,47] As expected, in APH-treated HEK293 cells, we found that FANCD2 colocalized with MiDAS (Figure 3A). Loss of GEN1 from HEK293 or U2OS cells did not impair FANCD2 localization or mono-ubiquitination (Figures 3A, S3A, and S3B). These results are consistent with previous studies showing that depletion of ERCC1 or MUS81 did not impact FANCD2 mono-ubiquitination, and that focus formation occurs independent of ATM and ATR activation.[28,31] Together, these data show that GEN1 and MUS81-EME1 promote SCG formation downstream of the role that FANCD2 plays in CFS maintenance.

Previous studies have shown that MiDAS at CFSs requires MUS81, EME1, and SLX4, indicating that MiDAS is dependent upon nucleolytic cleavage by MUS81-EME1.[29] To investigate whether the decrease of GEN1-mediated SCGs also led to a reduction in MiDAS, we exposed HEK293 and *GEN1* KO cells to APH followed by a 30-min pulse with EdU. We observed reduced MiDAS (measured by EdU incorporation) in mitotic *GEN1* KO cells compared with the WT control (Figures 3A and 3B). The reduction was similar to that observed in *MUS81* KO and double *GEN1 MUS81* KO cells (Figures 3A and 3B). These results indicate that the various nucleases promote SCG formation and CFS maintenance through a similar repair pathway. The reduction in MiDAS seen in the *GEN1* KO and *MUS81* KO cells was a direct consequence of the loss of the two nuclease activities (Figures 1A and 1B). Analysis of the remaining SCGs showed that the percentage of

replication fork. We found that, in contrast to PCNA, the binding of GEN1 to chromatin was not restricted to ongoing replication forks (Figures 2B and S2B). Similar results were observed with histone H3, which interacts with chromatin regardless of its replication status (Figure 2B). We observed no obvious difference in the association of GEN1 with chromatin upon APH treatment. These data show that although GEN1 is primarily cytoplasmic, there is a significant nuclear chromatin-bound fraction, giving rise to the possibility that it resolves replication intermediates prior to nuclear envelope breakdown.

In contrast to MUS81-EME1, which is specific for 3′ flap/fork structures,[43] GEN1 exhibits the opposite strand polarity and acts upon 5′ flap/fork structures.[41] The requirement for GEN1 may therefore reflect the need for a 5′ flap/fork endonuclease activity that complements the 3′ flap/fork activities of MUS81-EME1 and XPF-ERCC1. Because under-replicated DNA that arises after global replication stress would immediately be coated with replication protein A (RPA), we analyzed the activities of GEN1 and MUS81-EME1 on synthetic replication fork-like structures in the presence of RPA. Although RPA bound both the 5′ and 3′ flap/fork DNAs (Figures S2C and S2D), we found that its presence inhibited the 3′ flap/fork nuclease activity of MUS81-EME1, whereas it failed to inhibit the 5′ flap/fork activity of GEN1 to a similar extent (Figures 2C and 2D).

MUS81-EME1 activity peaks during prometaphase when it associates with SLX4 to form the SMX trinuclease.[33,43,46] Consistent with a role for SMX, MUS81-mediated CFS expression occurs in early mitosis.[29] We therefore determined whether purified SMX,
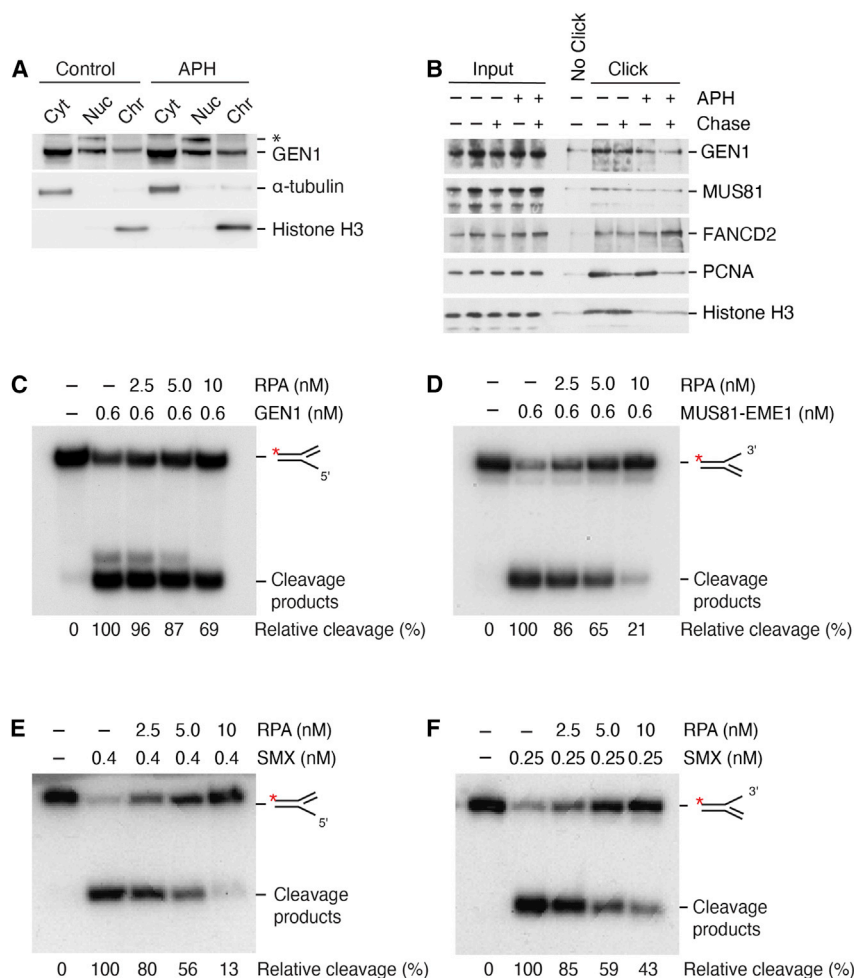
Figure 2. Nuclear GEN1 localizes to chromatin and cleaves RPA-coated replication fork-like structures

(A) Sub-cellular fractionation of HEK293 cells. Western blot analysis of cytoplasmic (Cyt), nuclear (Nuc), and chromatin (Chr) bound fractions following 24 h treatment with DMSO (control) or APH (0.4 μM). A cross-contaminating band, seen only in nuclear extracts, is indicated (*).

(B) iPOND analysis of HEK293 cells after treatment with APH (0.4 μM) or DMSO (control) for 18 h. Chase: 60-min incubation in thymidine-containing medium following 10 min EdU pulse. Input: 0.1% of whole cell lysate prior to streptavidin capture. Click: samples where Biotin was conjugated with nascent DNA. Controls: PCNA for association with the replication fork, histone H3 for chromatin, and MUS81 and FANCD2 for CFS.

(C) Cleavage of 5′ flap DNA, 5′ ^{32}P end labeled on one strand (asterisk) by GEN1. DNA was incubated with RPA prior to the addition of GEN1. Products were analyzed by native PAGE and visualized by autoradiography. Relative cleavage efficiency, quantified as a fraction of total cleavage observed in the absence of RPA, is indicated.

(D) As (C), except 3′ flap DNA was cleaved by MUS81-EME1.

(E) As (C), except 5′ flap DNA was cleaved by SMX.

(F) As (C), except 3′ flap DNA was cleaved by SMX.

See also Figure S2.

When MiDAS patterns were classified according to their presence on one or both sister chromatids, no significant differences were observed across all cell lines (Figure S3E). These results indicate that the DNA repair events that occur at SCGs are unlikely to be restricted to BIR occurring on a single chromatid.

SCGs undergoing MiDAS in the KO cells was similar to that observed in WT cells (Figures 3C and 3D). These results indicate that alternative endonucleases in the KO cells drive SCG formation and subsequent MiDAS events.

Previously, it was shown that MiDAS patterns on metaphase chromosomes are Pol δ dependent, and most EdU incorporation appears only on one of the two sister chromatids, indicative of a conservative BIR-like DNA repair mechanism.[48,49] However, these studies analyzed MiDAS on metaphase chromosomes regardless of the presence of a chromatid gap. We therefore analyzed the MiDAS focal patterns specifically associated with SCGs and found a highly dynamic repair process (Figures S3C and S3D). We classified a single focus as one focus on the gap or opposite the gap (Figure S3C, left). Double foci were classified as two foci flanking the gap on the same sister chromatid or one focus on each sister chromatid at the same allelic position (Figure S3C, center). These double foci were the more predominant pattern in HEK293 and *MUS81* KO cells but not in *GEN1* KO cells (Figure S3D). In addition, a number of SCGs exhibited three distinct loci that were associated with the gap and the sister chromatid opposite the gap (Figures S3C, right, and S3D).

MiDAS primarily involves Pol δ-dependent repair

POLD1 and POLD3 are the catalytic and accessory subunits of Pol δ, respectively, and localize with MUS81-EME1 to chromatin upon replication stress. Depletion of POLD3 resulted in decreased SCGs and MiDAS, consistent with a role for Pol δ in mediating BIR repair synthesis.[29] To determine whether Pol δ plays the same role in WT, *GEN1* KO, and *MUS81* KO cells, we depleted POLD1 or POLD3 (Figure S3F) and measured SCGs and MiDAS. As expected, WT cells depleted for POLD1 or POLD3 exhibited fewer SCGs (Figure 3E) and a corresponding reduction in MiDAS (Figure 3F). We therefore analyzed for more subtle changes to MiDAS and found that depletion of POLD3 from WT, *GEN1*, or *MUS81* KOs did not affect the overall frequency of MiDAS at SCGs (Figure 3G). However, MiDAS involving two sister chromatids decreased in the *MUS81* KO but not in the *GEN1* KO or WT cells following POLD3 depletion (Figures S3G–S3J). In contrast, depletion of POLD1 decreased MiDAS at SCGs in WT and *MUS81* KO cells but not in the *GEN1* KOs (Figure 3G). These differences were specifically
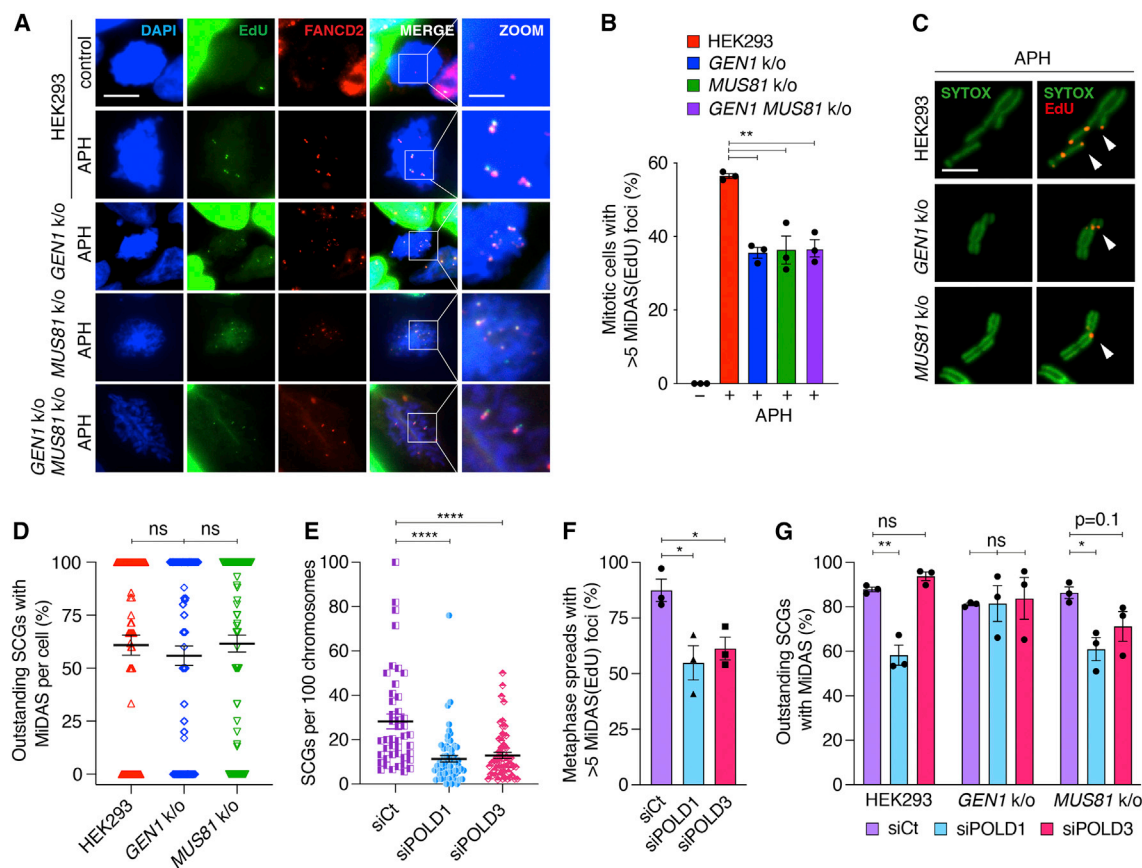
Figure 3. *GEN1*-defective cells exhibit reduced MiDAS

(A) Representative immunofluorescence images of HEK293, *GEN1* KO, *MUS81* KO, and *GEN1 MUS81* KO cells treated with APH (0.4 μM) or DMSO (control) for 24 h. The colocalization of MiDAS (EdU, green) with FANCD2 (red) in mitotic nuclei (DAPI, blue) is shown. Scale bars: 15 μm and 5 μm (zoom).

(B) Mitotic cells with >5 EdU/FANCD2 foci were quantified, as in (A). 166 HEK293, 181 HEK293, 186 *GEN1* KO, 226 *MUS81* KO, and 129 *GEN1 MUS81* KO cells were scored. APH (0.4 μM) was used where indicated. Data are represented as mean ± SEM; n = 3.

(C) Representative images of SCGs in HEK293, *GEN1* KO, and *MUS81* KO cells after APH treatment (0.4 μM, 24 h). MiDAS is represented by EdU (red) incorporation during 30 min pulse treatment prior to spreading. Chromosomes were stained with SYTOX-green. Scale bar: 2.5 μm.

(D) Quantification of the distribution of MiDAS-positive SCGs, as in (C). 83 HEK293, 93 *GEN1* KO, and 120 *MUS81* KO cells were scored. Data are represented as mean ± SEM; n = 3.

(E) Quantification of SCGs per 100 chromosomes in HEK293 cells targeted with siControl (44 cells), siPOLD1 (60 cells), or siPOLD3 (60 cells). Data are represented as mean ± SEM; n = 3.

(F) Percentage of mitotic spreads with >5 EdU/FANCD2 foci were quantified in HEK293 cells targeted with siControl (102 cells), siPOLD1 (127 cells), or siPOLD3 (118 cells) RNA. Data are represented as mean ± SEM; n = 3.

(G) Quantification of MiDAS on the observed SCGs in HEK293, *GEN1* KO, and *MUS81* KO cells depleted for POLD1 and POLD3. Approximately 200 SCGs were scored per condition. Data are represented as mean ± SEM; n = 3. See also Figure S3.

found at MiDAS events involving two sister chromatids (Figures S3H and S3J). These results show that the precise MiDAS arrangements and reliance on Pol δ differ according to the nuclease that drives SCG formation.

GEN1 loss leads to ultrafine DNA bridge formation during anaphase

At anaphase, under-replicated DNA promotes the formation of DAPI-negative ultrafine DNA bridges (UFBs) that are coated with BLM helicase, PICH (Plk1-interacting checkpoint helicase), and RPA.[28,50] At this stage of mitosis, the FANCD2 twin foci separate, so each focus is located at a similar position in the two daughter cells. FANCD2-positive UFBs that arise from

CFS loci are generally present in unchallenged cells and increase upon replication stress and/or depletion of MUS81. These observations indicate that UFB formation is a direct consequence of defects in CFS expression and MiDAS.[30,50]

We therefore determined whether loss of GEN1 exacerbated UFB formation following replication stress and observed that unchallenged and APH-treated *GEN1* KO U2OS cells exhibited a large increase in the number of anaphase cells with RPA-coated UFBs flanked by FANCD2 (Figures 4A and 4B). Moreover, the total number of bridges linking the two separating DNA masses was significantly increased in the *GEN1* KO cells (Figure 4A). Similar results were observed in *GEN1* KO HEK293 cells (Figures S4A–S4C). The average number of bridges was significantly greater in the
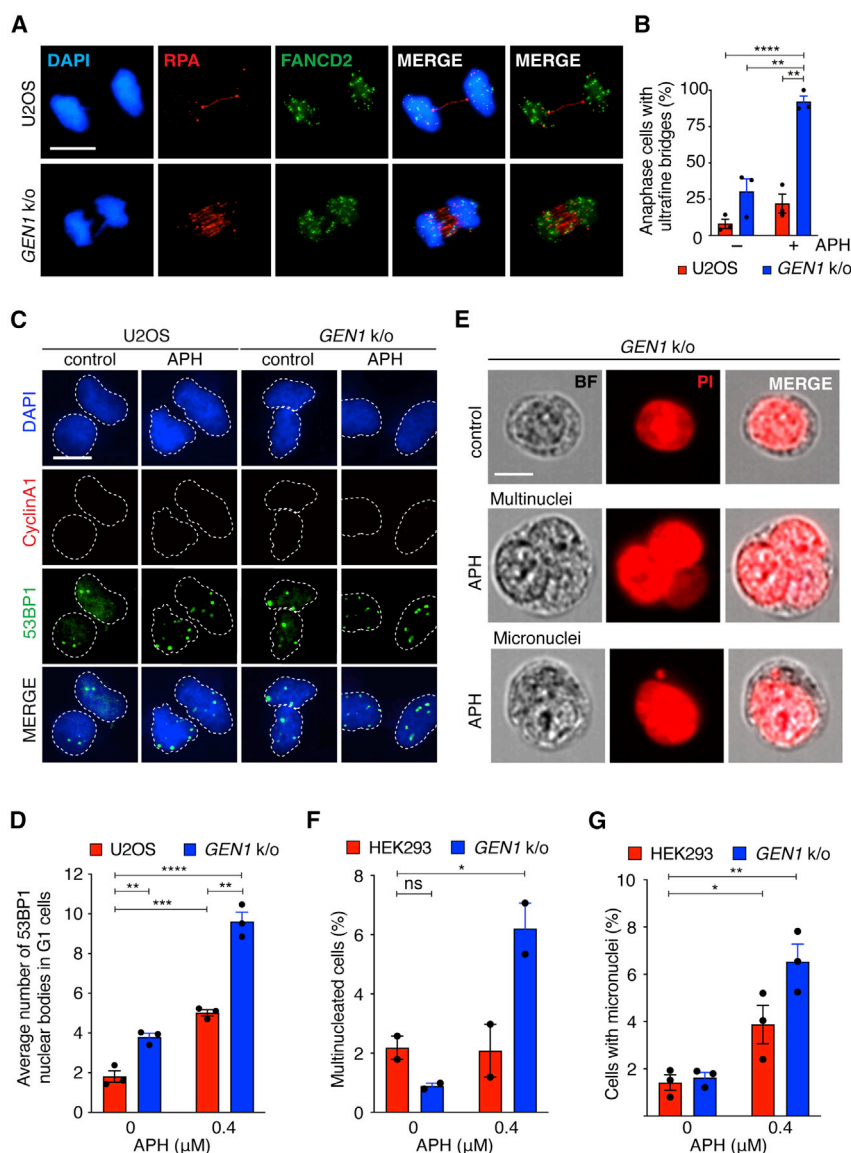
Figure 4. Replication stress in *GEN1*-defective cells promotes increased UFB formation, 53BP1 G1 nuclear bodies, multinucleation, and micronucleation

(A) U2OS and *GEN1* KO cells were treated with APH (0.4 μM, 24 h). Representative images of anaphase cells show UFBs coated with RPA (red) and flanked by FANCD2 foci (green). Scale bar: 8.8 μm.

(B) Quantification of anaphase cells with RPA-coated UFBs flanked by FANCD2 twin foci, as in (A). 171 HEK293, 151 HEK293 (APH), 160 *GEN1* KO (DMSO), and 161 *GEN1* KO (APH) cells were analyzed.

(C) Representative images of U2OS and *GEN1* KO cells in G1 (cyclin A1 negative) showing 53BP1 nuclear bodies (green) after APH treatment (0.4 μM). DNA is stained with DAPI (blue), with cyclin A1 in red. Scale bar: 15 μm.

(D) Quantification of 53BP1 nuclear bodies in (C). 300 cells were scored per condition. Data are represented as mean ± SEM; n = 3. Scale bars: 15 μm.

(E) Representative ImageStream images of normal, multinucleated, and micronucleated G1 phase *GEN1* KOs following treatment with APH (0.4 μM, 24 h) or DMSO (control). Scale bar: 7 μm.

(F) Quantification of multinucleated HEK293 and *GEN1* KO cells after treatment with APH (0.4 μM) or DMSO (control). 1,007 HEK293 (DMSO), 1,005 HEK293 (APH), 1,007 *GEN1* KO (DMSO), and 2,015 *GEN1* KO (APH) cells were analyzed. Data are represented as mean ± SEM; n = 2.

(G) Quantification of HEK293 and *GEN1* KO cells with >1 micronucleus after treatment with APH (0.4 μM) or DMSO. 2,490 HEK293 (DMSO), 1,282 HEK293 (APH), 4,205 *GEN1* KO (DMSO), and 4,800 *GEN1* KO (APH) cells were analyzed. Data are represented as mean ± SEM; n = 3. See also Figure S4.

GEN1 KO compared with the *MUS81* KO cell line (Figure S4B). Examination of the RPA-coated UFBs revealed that most were flanked by FANCD2 foci and represent sites of unresolved replication intermediates and fragile site bridging (Figures S4C).

Although APH treatment also leads to the formation of DAPI-positive bulky bridges and lagging chromosomes, we did not observe any significant differences between the HEK293 and *GEN1* KO cells (Figures S4D and S4E), in contrast to MUS81-EME1 depletion that increases bulky bridge formation.[30,51] These data indicate that although GEN1 and MUS81-EME1 promote CFS expression, the lack of either nuclease may lead to distinct anaphase outcomes.

GEN1 KOs exhibit 53BP1 nuclear body formation, multinucleation, and micronucleation

A failure to disentangle DNA linkages poses a severe threat to mitosis and genome stability. Defects in CFS expression and repair therefore result in a variety of abnormal phenotypes in the ensuing G1 phase of daughter cells including (1) the formation of large 53BP1 nuclear bodies as a consequence of DNA breakage,[2,52–54] (2) multinucleation, which may result from an increased number of chromosome bridges and cytokinesis failure,[31,55] and (3) micronucleation, which may arise as a consequence of aberrant anaphase bridge breakage.[56]

When *GEN1* KO U2OS cells were compared with WT controls, we observed increased 53BP1 nuclear body formation, and these levels increased following APH treatment (Figures 4C and 4D). Similar results were obtained in HEK293 cells (Figures S4F and S4G). These results indicate that, in the absence of GEN1, aberrant bridge breakage leads to DNA damage that persists into the second cell cycle. Similar results have been observed following siRNA-mediated depletion of MUS81 or ERCC1.[31]

To examine the effect of GEN1 loss on multinucleation, we analyzed over 4,000 cells using image-based flow cytometry. A mitotic-specific marker, MPM2,[57] was used to exclude cells that were actively undergoing cellular division (Figure S4H). We found that *GEN1* KO HEK293 cells exhibited a significant

increase in multinucleation after replication stress, with >6% of the cells multinucleated (Figures 4E and 4F), suggesting that increased bridging leads to cytokinesis failure and multinucleation. Similarly, we found that APH-induced replication stress resulted in an increased frequency of micronucleation, which was exacerbated in the *GEN1* KOs (Figures 4E and 4G). Previously, it was shown that depletion of MUS81 led to increased micronuclei, and these were found to associate with known CFS loci.[30]

Together, these data show that in the absence of GEN1, replication-stress-induced CFS bridging leads to abnormal G1 phenotypes in daughter cells. This is consistent with previous findings with MUS81 depletion[29–31] and provides further support for a role for GEN1 in CFS maintenance.

Effect of GEN1 and MUS81 loss on copy number variation

Aberrant repair of persistent replication intermediates can lead to genomic gain/amplification and loss/deletion events, the latter of which can cause loss of heterozygosity in daughter cells, a hallmark of CFSs. To determine whether loss of GEN1 affected the frequency of amplification/deletion events, we used lenti-CRISPRv2 to derive KOs from a single U2OS clone targeted with *GEN1* sgRNA, *MUS81* sgRNA, or a non-targeting control (NTC). To ensure that cells progressed through the cell cycle with only mild replication stress, we used a low dose of APH (0.2 μM) and a longer treatment time (48 h). Cells were subsequently released from APH, allowed to recover for 24 h, and then expanded into single cell clones in order to amplify any genomic changes incurred during drug treatment. The KO efficiency of each clone was then analyzed by western blotting (Figure S5A) prior to copy number variation (CNV) analyses. FRA10D, FRA16D, and FRA3B were chosen for their high frequency of breakage and strong association with MiDAS upon replication stress in U2OS cells.[58] *SEMA6D*, a long non-fragile gene in chromosome 15, was used as a control.

We analyzed three independent NTC untreated clones, four that were APH treated, three untreated *GEN1* KO clones, two APH-treated *GEN1* KO clones, four untreated *MUS81* KO clones, and four APH-treated *MUS81* KO clones. At FRA10D, which harbors the *NRG3* locus, 1/3 of the untreated NTC clones showed a significant increase in CNV, although the magnitude of CNV was quite small (Figures S5B and S6A). In contrast, 3/4 of the APH-treated NTC clones showed significantly increased CNV (Figures S5B and S6A). The overall magnitude of CNV was higher after APH treatment. Similar findings were observed in FRA16D (*WWOX*), to a lesser extent at FRA3B (*FHIT*), but not in *SEMA6D* (Figures S5C–S5E and S6B–S6D). When the *GEN1* KO and *MUS81* KO clones were analyzed, with or without APH treatment, we did not observe increased instability (Figures S5B–S5E and S6A–S6D). Similar results were obtained with prolonged APH treatment, although as expected the dose of APH was inversely correlated with cellular viability in WT, *GEN1* KO, and *MUS81* KO cells (Figures S6E and 6F).

GEN1 loss promotes increased BCG formation and chromosome segmentation

BCGs or constrictions represent undercondensed regions of the chromosome that do not stain with Giemsa, DAPI, or condensins

such as SMC2[59] and that can arise from sister-chromatid entanglements caused by the presence of unresolved recombination intermediates.[54,59] These constrictions lead to a segmentation phenotype and were particularly evident in BLM-deficient cells depleted of MUS81 and GEN1, or SLX4 and GEN1, following mild DNA damage.[59,60] Abnormally condensed chromosomes, exhibiting a segmentation phenotype, have also been observed in *Drosophila* mutated for components of the origin recognition complex (ORC),[61,62] as well as in HeLa and RPE1 cells treated with APH,[18,28] indicating that persistent unresolved replication intermediates at CFSs may be an additional source of constrictions.

Analysis of metaphase spreads from APH-treated HEK293 *GEN1* KO cells revealed a significant increase in constrictions/segmentation compared with WT cells (Figures 5A and 5B). Double *GEN1 MUS81* KO cells also showed an increase in constrictions upon replication stress, although the *MUS81* KO alone did not. Similar results were obtained in siRNA-depleted U2OS cells (Figures S7A–S7C). These data indicate that although CFS expression can be driven by both nucleases, GEN1 loss in particular leads to increased BCGs or constrictions at genomic loci.

BCGs are repaired via POLD1-dependent MiDAS

To determine whether BCGs, like SCGs, undergo MiDAS, we visualized metaphase chromosomes from cells that were pulse labeled with EdU for 30 min immediately before spread preparation. As observed with SCGs, the BCGs incorporated EdU during mitosis, and loss of GEN1 or MUS81 did not impair the overall frequency of MiDAS (Figures 5C and 5D). These data indicate that despite their increased appearance under conditions of replication stress, BCGs also undergo a last-minute attempt at DNA repair during mitosis.

Detailed analysis of the different MiDAS focal patterns at BCGs indicates a dynamic repair process (Figures 6A–6C and S8A) reminiscent of the MiDAS observed at SCGs (Figures S3A and S3B).[48] The most predominant MiDAS arrangement in WT, *GEN1* KO, and *MUS81* KO cells was double foci (Figure 6D). More extensive MiDAS was observed on some occasions where both sister chromatids in a BCG were joined by EdU incorporation (Figure S8A). We also observed MiDAS at seemingly unperturbed regions where no cytogenetic gaps were present (Figure S8B).

As with SCGs, MiDAS at BCGs was dependent on POLD1, but not POLD3, in WT and *MUS81* KO cells (Figure 6E). POLD1 depletion in these cells only affected the ability for MiDAS to occur on both sister chromatids (Figures S8D and S8E). In contrast, in the *GEN1* KO cells, MiDAS within BCGs appeared to take place by a POLD1/POLD3-independent mechanism (Figure 6E). However, upon closer inspection, we observed that depletion of POLD1 decreased MiDAS involving two sister chromatids and increased MiDAS involving one sister chromatid (Figure S8F). Overall, BCG formation was not affected by the absence of POLD1 or POLD3 (Figure S8C). These findings indicate that while BCGs may undergo similar MiDAS-dependent repair mechanisms as SCGs, they can arise under different conditions independently of POLD1, POLD3, or MUS81-EME1.
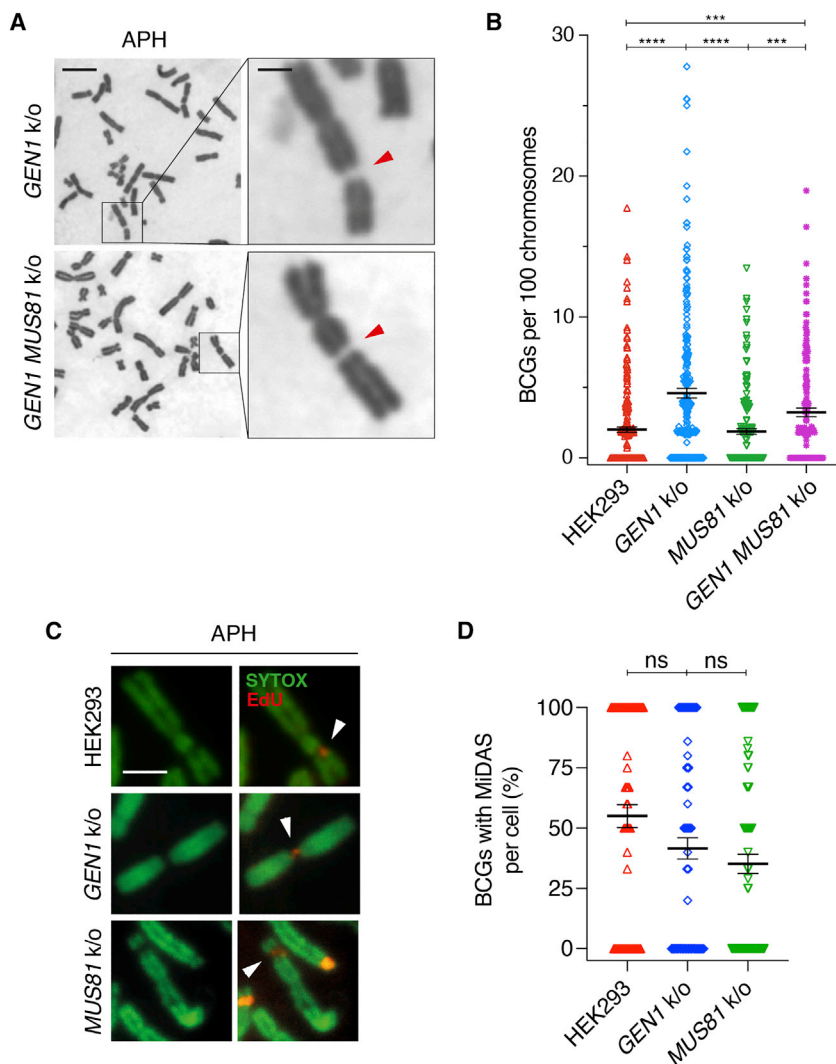
Figure 5. *GEN1*-defective cells exhibit increased bichromatid gaps following replication stress

(A) Representative images of Giemsa-stained metaphase chromosome spreads of *GEN1* KO and *GEN1 MUS81* KO cells after treatment with aphidicolin (0.4 μM, 24 h). Red arrows indicate BCGs. Scale bars: 5 μm and 1 μm (zoom).

(B) Quantification of the number of BCGs per 100 chromosomes, as in (A). 240 HEK293, 240 *GEN1* KO, 180 *MUS81* KO, and 150 *GEN1 MUS81* KO cells were scored. Data are represented as mean ± SEM; n = 3.

(C) Representative images of BCGs in HEK293, *GEN1* KO, and *MUS81* KO cells after APH treatment (0.4 μM, 24 h). MiDAS is represented by EdU (red) incorporation during 30-min pulse treatment prior to spreading. Chromosomes are stained with SYTOX-green. Scale bar: 2.5 μm.

(D) Quantification of the distribution of MiDAS-positive BCGs, as in (C). 87 HEK293, 97 *GEN1* KO, and 106 *MUS81* KO cells were scored. Data are represented as mean ± SEM; n = 3. See also Figure S7.

may reflect a need for a 5′ flap/fork endonuclease activity to complement the 3′ flap/fork nucleases MUS81-EME1 and XPF-ERCC1. Additionally, *in vitro* experiments with the purified nucleases revealed that the single-strand binding protein RPA inhibited the cleavage of model replication forks by MUS81-EME1 and the SMX complex but had a lesser effect on GEN1. One possibility is that the incision of RPA-bound forks may be favored by the small size of GEN1 (100 kDa), which contrasts with the much larger SMX complex (estimated to be around 1 MDa).

As observed with MUS81-EME1 deficient cells, decreased SCG formation during early mitosis in the *GEN1* KO cells was associated with decreased MiDAS. This decrease was a direct consequence of reduced SCG formation. However, depletion of either endonuclease did not affect the ability of the remaining SCGs to undergo MiDAS, indicating that other nucleases are still able to target these loci and produce SCGs that undergo MiDAS repair.

Previous studies showed that *de novo* DNA synthesis through MiDAS was a POLD3-dependent mechanism.[29] However, in WT and *MUS81* KO cells, we found that depletion of POLD1 but not POLD3 resulted in impaired MiDAS at SCGs, in particular when MiDAS was observed on both sister chromatids. We suggest that the apparent dependence of MiDAS on POLD3, as reported previously, may be due to the global decrease in MiDAS observed upon POLD3 depletion, which in turn is a direct consequence of a decrease in SCGs. Indeed, POLD3 and POLD1 may play a role upstream of SCG formation, which is different from the role played in MiDAS. Consistent with this, POLD3 and POLD4 are required for cell cycle progression and fork processivity upon oncogene-induced replication stress.[38] Interestingly,
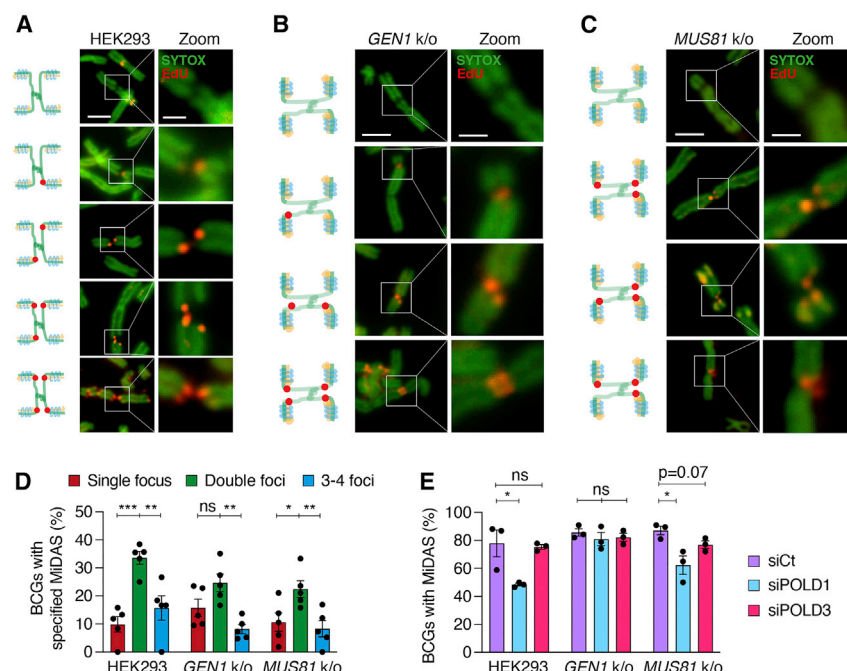
DISCUSSION

The contribution of MUS81-EME1 and XPF-ERCC1 to CFS expression is well characterized. In the absence of these nucleases, under-replicated DNA at CFS loci impacts mitotic chromosome segregation, visualized by the formation of unresolved ultrafine bridges, leading to DNA damage in the resulting G1 cells and increased genome instability. Here, we show that GEN1 nuclease, which was formerly thought to be required primarily for the resolution of recombination intermediates, provides an additional mechanism for CFS expression. GEN1 therefore plays a dual role, resolving both DNA replication and recombination intermediates prior to chromosome segregation. The loss of both GEN1 and MUS81-EME1 activity did not result in a further reduction in mitotic CFS expression, indicating that the SMX-associated nucleases and GEN1 may have similar target substrates and/or work in parallel to maintain genomic integrity at CFSs.

Our results indicate that GEN1 and MUS81-EME1 contribute equally toward CFS maintenance. The requirement for GEN1

Figure 6. Repair of bichromatid gaps by MiDAS

(A) Representative images of HEK293 cells after treatment with APH (0.4 μM, 24 h) showing BCGs undergoing MiDAS during metaphase. Schematics illustrate MiDAS arrangements. MiDAS is represented by EdU (red) incorporation during a 30-min pulse treatment prior to metaphase spread preparation. Chromosomes are stained with SYTOX-green. Scale bars: 2.5 μm and 0.8 μm (zoom).

(B) As in (A), except *GEN1* KO cells.

(C) As in (A), except *MUS81* KO cells.

(D) Quantification of MiDAS arrangements within BCGs as in (A), (B), and (C).

(E) Quantification of MiDAS on BCGs in HEK293, *GEN1* KO, and *MUS81* KO cells depleted for POLD1. Approx 95 BCGs were scored per condition. Data are represented as mean ± SEM; n = 3. See also Figure S8.

many cancers overexpress POLD3, as well as MUS81, GEN1, RAD1, and MLH1, which hints toward an increased reliance on these proteins in cancer cells, where oncogene-induced replication stress may be elevated.[63,64] In *MUS81* KO cells, POLD1 and POLD3 depletion resulted in decreased MiDAS at BCGs, whereas there was some evidence for POLD1/POLD3-independent MiDAS in *GEN1* KO cells. These results indicate that MiDAS is dependent upon the nuclease that promotes cleavage, which in turn directs the polymerase that initiates repair. As such, the POLD1-dependent MiDAS observed in WT cells may result from SCGs formed primarily by GEN1 rather than MUS81.

In APH-treated *GEN1* KOs, we found that UFB formation was greatly elevated. Moreover, the average number of bridges in each cell was increased in comparison with WT or *MUS81* KO cells. A different situation is evident in yeast cells disrupted for Yen1, as increased breakage at the FLEX1 locus was observed, whereas loss of Mus81, Slx1, and Slx4 led to decreased breakage.[39] One possibility is that *yen1* mutants accumulate secondary structures at, or close to, slowed replication forks and that these serve as substrates for Mus81/Mms4 or Slx1/Slx4. It is unlikely that similar events occur in mammalian cells, since decreased SCG formation was observed in the absence of GEN1 or MUS81-EME1.

The mitotic defects found in *GEN1* KO cells were carried through to the next cell cycle, where we observed increased numbers of 53BP1 nuclear bodies in G1 cells, presumably due to aberrant bridge breakage. We also observed increased multi-nucleation and micronucleation events typical of defective mitosis. Together, our findings with GEN1 are consistent with previous work on MUS81-EME1 and XPF-ERCC1 and support the theory that all three nucleases promote repair at CFSs.

Despite the striking short-term phenotypes seen in APH-treated *GEN1* KO cells, we did not observe increased genomic

instability at three different CFS loci when compared with WT cells. Comparable results were obtained from *MUS81* KO cells. However, these CNV observations must be tempered with the caveat that prolonged APH treatment causes decreased cell viability, and it is possible that this reduction masks any instability that occurs due to reduced CFS expression. Similarly, we did not observe any significant differences in cellular viability when isogenic WT, *GEN1* KO, and *MUS81* KO cells were compared under conditions where there was chronic induction of replication stress, suggesting that the KOs maintain a robust DNA repair response.

In contrast to the *MUS81* KO cells, exposure of the *GEN1* KOs to replication stress led to BCGs, visualized on metaphase spreads as a segmentation phenotype. Similar BCGs have been observed in *Drosophila* mutants defective for components of the origin recognition complex[61,62] and in Holliday junction resolvase-deficient cells treated with DNA damaging agents.[59,60,65] These results indicate that BCGs arise as a consequence of unresolved replication or recombination intermediates. Both types of BCGs give rise to UFBs at anaphase, with one significant difference in that the replication-induced UFB (FS-UFBs) are marked by FANCD2 foci whereas the recombination UFBs (HR-UFBs) are not.[54]

While SCGs are thought to be a direct consequence of nucleolytic action, APH-induced BCGs appear to be regions of uncondensed DNA. SCGs and BCGs cannot be stained with Giemsa, DAPI, or antibodies against the condensin protein SMC2.[59] BCGs are also characterized by the colocalization of FANCD2 and γH2AX, despite the apparent absence of endonucleolytic cleavage.[28] As observed with SCGs, however, the BCGs undergo MiDAS as a last resort in an attempt to complete replication in time for cell division. In WT and *MUS81* KO cells, where BCGs are rare, they undergo POLD1-dependent MiDAS. In contrast, in GEN1 KO cells, where BCGs are increased, they can undergo POLD1/POLD3-independent MiDAS mechanism. In accord with these results, APH treatment of cells depleted for condensin I and condensin II also

results in increased cytogenetic lesions and corresponding MiDAS,[18] supporting the theory that under-condensed DNA undergoes MiDAS as a last-minute attempt to rescue the aberrant phenotype. However, whether BCGs invoke alternative nucleolytic cleavage activities prior to initiating MiDAS remains to be determined.

The inherent potential for CFS instability in healthy individuals and its link to early stages of tumor development underpins the importance of understanding the molecular mechanisms of fragile site maintenance. We propose here a model whereby under-replicated DNA intermediates at fragile sites are marked by FANCD2 prior to their nuclease-mediated cleavage driven by GEN1, MUS81-EME1, XPF-ERCC1, or the SMX trinuclease complex. Cleavage is then followed by MiDAS, which attempts to rescue replication and allow mitotic division. In the absence of cleavage and MiDAS, cells will instead accumulate under-replicated DNA intermediates that manifest as FS-UFBs at anaphase. Following GEN1 loss, a fraction of the GEN1-specific target sites are realized as chromosome constrictions during metaphase but ultimately undergo last-minute DNA repair through MiDAS.

In summary, cells have robust DNA repair mechanisms that act in response to replication stress, and most unresolved intermediates will be processed by the variety of endonucleases that are available. In rare occasions, however, when anaphase bridging is too high, as a consequence of replication stress, cell division may ultimately fail, leading to multinucleated or micronucleated cells, while others may accumulate G1-specific phenotypes such as breaks marked by 53BP1 foci. Such abnormalities are likely to underscore the reason why CFSs represent hotspots for cancer-specific chromosomal aberrations such as deletions, amplifications, and translocations.

Limitations of the study

We find that GEN1 promotes fragile site expression. In the absence of GEN1, cells exhibit the formation of SCGs and BCGs. Since many of the experiments involve the cytogenetic analysis of metaphase spreads, the observations are primarily descriptive, and further experiments are required to determine the mechanistic role played by GEN1. It is presently unclear whether the SCGs represent chromosome breaks or regions where incomplete condensation takes place, and this warrants further investigation. SCGs may be breaks driven by nucleases, which decrease in the absence of GEN1 or MUS81, whereas BCGs are thought to be uncondensed regions of DNA that increase in the absence of GEN1 but not MUS81. The present work makes no attempt to determine whether the SCGs and BCGs occur within the proximity of cytogenetically mapped CFS loci, only that they are induced by treatment with APH. Although MiDAS was observed in chromatid gaps and was found to be dependent, at least in part, on Pol δ, other polymerases are likely to be involved. These may vary according to the nuclease that promotes DNA cleavage. In this study we did not find evidence of CNV in the *GEN1* or *MUS81* KO cells relative to WT. However, the CNV observations are tempered with the caveat that prolonged APH treatment causes decreased cell viability, and it is possible that this reduction masks any instability that occurs.

STAR★METHODS

Detailed methods are provided in the online version of this paper and include the following:

- KEY RESOURCES TABLE
- RESOURCE AVAILABILITY
  - Lead contact
  - Materials availability
  - Data and code availability
- EXPERIMENTAL MODEL AND SUBJECT DETAILS
  - Cell lines
- METHOD DETAILS
  - Pool lentiviral CRISPR knockout
  - Single cell CRISPR knockout
  - siRNA interference
  - Metaphase chromosome spreads
  - Immunofluorescence on chromosome spreads
  - Immunofluorescence
  - Flow cytometry
  - Subcellular fractionation
  - Isolation of proteins on nascent DNA (iPOND)
  - Western blotting
  - Expression and purification of proteins
  - DNA cleavage reactions
  - Electrophoretic mobility shift assay (EMSA)
  - Imagestream analysis of micronucleation and multinucleation
  - Cell viability and survival
  - Copy number variation (CNV)
- QUANTIFICATION AND STATISTICAL ANALYSIS
  - Statistical analysis

Cell Reports
Article

REFERENCES

1. Glover, T.W., Berger, C., Coyle, J., and Echo, B. (1984). DNA polymerase α inhibition by aphidicolin induces gaps and breaks at common fragile sites in human chromosomes. Hum. Genet. *67*, 136–142. https://doi.org/10.1007/BF00272988.

2. Lukas, C., Savic, V., Bekker-Jensen, S., Doil, C., Neumann, B., Pedersen, R.S., Grøfte, M., Chan, K.L., Hickson, I.D., Bartek, J., and Lukas, J. (2011). 53BP1 nuclear bodies form around DNA lesions generated by mitotic transmission of chromosomes under replication stress. Nat. Cell Biol. *13*, 243–253. https://doi.org/10.1038/ncb2201.

3. Glover, T.W., Wilson, T.E., and Arlt, M.F. (2017). Fragile sites in cancer: more than meets the eye. Nat. Rev. Cancer *17*, 489–501. https://doi.org/10.1038/nrc.2017.52.

4. Debatisse, M., Le Tallec, B., Letessier, A., Dutrillaux, B., and Brison, O. (2012). Common fragile sites: mechanisms of instability revisited. Trends Genet. *28*, 22–32. https://doi.org/10.1016/j.tig.2-11.10.003.

5. Brison, O., El-Hilali, S., Azar, D., Koundrioukoff, S., Schmidt, M., Nähse, V., Jaszczyszyn, Y., Lachages, A.M., Dutrillaux, B., Thermes, C., et al. (2019). Transcription-mediated organization of the replication initiation program across large genes sets common fragile sites genome-wide. Nat. Commun. *10*, 5693. https://doi.org/10.1038/s41467-019-13674-5.

6. Miron, K., Golan-Lev, T., Dvir, R., Ben-David, E., and Kerem, B. (2015). Oncogenes create a unique landscape of fragile sites. Nat. Commun. *6*, 7094. https://doi.org/10.1038/ncomms8094.

7. Kumar, R., Nagpal, G., Kumar, V., Usmani, S.S., Agrawal, P., and Raghava, G.P.S. (2019). HumCFS: a database of fragile sites in human chromosomes. BMC Genom. *19*, 985. https://doi.org/10.1186/s12864-018-5330-5.

8. Blin, M., Le Tallec, B., Nähse, V., Schmidt, M., Brossas, C., Millot, G.A., Prioleau, M.N., and Debatisse, M. (2019). Transcription-dependent regulation of replication dynamics modulates genome stability. Nat. Struct. Mol. Biol. *26*, 58–66. https://doi.org/10.1038/s41594-018-0170-1.

9. Wilson, T.E., Arlt, M.F., Park, S.H., Rajendran, S., Paulsen, M., Ljungman, M., and Glover, T.W. (2015). Large transcription units unify copy number variants and common fragile sites arising under replication stress. Genome Res. *25*, 189–200. https://doi.org/10.1101/gr.177121.114.

10. Le Tallec, B., Millot, G.A., Blin, M.E., Brison, O., Dutrillaux, B., and Debatisse, M. (2013). Common fragile site profiling in epithelial and erythroid cells reveals that most recurrent cancer deletions lie in fragile sites hosting large genes. Cell Rep. *4*, 420–428. https://doi.org/10.1016/j.celrep.2013.07.003.

11. Glover, T.W., Arlt, M.F., Casper, A.M., and Durkin, S.G. (2005). Mechanisms of common fragile site instability. Hum. Mol. Genet. *14*, R197–R205. https://doi.org/10.1093/hmg/ddi265.

12. Macheret, M., Bhowmick, R., Sobkowiak, K., Padayachy, L., Mailler, J., Hickson, I.D., and Halazonetis, T.D. (2020). High-resolution mapping of mitotic DNA synthesis regions and common fragile sites in the human genome through direct sequencing. Cell Res. *30*, 997–1008. https://doi.org/10.1038/s41422-020-0358-x.

13. Letessier, A., Millot, G.A., Koundrioukoff, S., Lachagès, A.M., Vogt, N., Hansen, R.S., Malfoy, B., Brison, O., and Debatisse, M. (2011). Cell-type-specific replication initiation programs set fragility of the FRA3B fragile site. Nature *470*, 120–123. https://doi.org/10.1038/nature09745.

14. Le Beau, M.M., Rassool, F.V., Neilly, M.E., Espinosa, R., 3rd, Glover, T.W., Smith, D.I., and McKeithan, T.W. (1998). Replication of a common fragile site, FRA3B, occurs late in S phase and is delayed further upon induction: implications for the mechanism of fragile site induction. Hum. Mol. Genet. *7*, 755–761. https://doi.org/10.1093/hmg/7.4.755.

15. Hellman, A., Rahat, A., Scherer, S.W., Darvasi, A., Tsui, L.C., and Kerem, B. (2000). Replication delay along FRA7H, a common fragile site on human chromosome 7, leads to chromosomal instability. Mol. Cell Biol. *20*, 4420–4427. https://doi.org/10.1128/MCB.20.12.4420-4427.2000.

16. Sarni, D., Sasaki, T., Irony Tur-Sinai, M., Miron, K., Rivera-Mulia, J.C., Magnuson, B., Ljungman, M., Gilbert, D.M., and Kerem, B. (2020). 3D genome organization contributes to genome instability at fragile sites. Nat. Commun. *11*, 3613. https://doi.org/10.1038/s41467-020-17448-2.

17. Jiang, Y., Lucas, I., Young, D.J., Davis, E.M., Karrison, T., Rest, J.S., and Le Beau, M.M. (2009). Common fragile sites are characterized by histone hypoacetylation. Hum. Mol. Genet. *18*, 4501–4512. https://doi.org/10.1093/hmg/ddp410.

18. Boteva, L., Nozawa, R.S., Naughton, C., Samejima, K., Earnshaw, W.C., and Gilbert, N. (2020). Common fragile sites are characterized by faulty condensin loading after replication stress. Cell Rep. *32*, 108177. https://doi.org/10.1016/j.celrep.2020.108177.

19. Irony-Tur Sinai, M., Salamon, A., Stanleigh, N., Goldberg, T., Weiss, A., Wang, Y.H., and Kerem, B. (2019). AT-dinucleotide rich sequences drive fragile site formation. Nucleic Acids Res. *47*, 9685–9695. https://doi.org/10.1093/nar/gkz689.

20. Zlotorynski, E., Rahat, A., Skaug, J., Ben-Porat, N., Ozeri, E., Hershberg, R., Levi, A., Scherer, S.W., Margalit, H., and Kerem, B. (2003). Molecular basis for expression of common and rare fragile sites. Mol. Cell Biol. *23*, 7143–7151. https://doi.org/10.1128/MCB.23.20.7143-7151.2003.

21. Burrow, A.A., Marullo, A., Holder, L.R., and Wang, Y.H. (2010). Secondary structure formation and DNA instability at fragile site FRA16B. Nucleic Acids Res. *38*, 2865–2877. https://doi.org/10.1093/nar/gkp1245.

22. Zhang, H., and Freudenreich, C.H. (2007). An AT-rich sequence in human common fragile site FRA16D causes fork stalling and chromosome breakage in S. cerevisiae. Mol. Cell *27*, 367–379. https://doi.org/10.1016/j.molcel.2007.06.012.

23. Baranovskiy, A.G., Babayeva, N.D., Suwa, Y., Gu, J., Pavlov, Y.I., and Tahirov, T.H. (2014). Structural basis for inhibition of DNA replication by aphidicolin. Nucleic Acids Res. *42*, 14013–14021. https://doi.org/10.1093/nar/gku1209.

24. Palakodeti, A., Lucas, I., Jiang, Y., Young, D.J., Fernald, A.A., Karrison, T., and Le Beau, M.M. (2010). Impaired replication dynamics at the FRA3B common fragile site. Hum. Mol. Genet. *19*, 99–110. https://doi.org/10.1093/hmg/ddp470.

25. Brosh, R.M., Jr., Bellani, M., Liu, Y., and Seidman, M.M. (2017). Fanconi Anemia: a DNA repair disorder characterized by accelerated decline of the hematopoietic stem cell compartment and other features of aging. Ageing Res. Rev. *33*, 67–75. https://doi.org/10.1016/j.arr.2016.05.005.

26. Niraj, J., Färkkilä, A., and D'Andrea, A.D. (2019). The Fanconi anemia pathway in cancer. Annu. Rev. Cancer Biol. *3*, 457–478. https://doi.org/10.1146/annurev-cancerbio-030617-050422.

27. Howlett, N.G., Taniguchi, T., Durkin, S.G., D'Andrea, A.D., and Glover, T.W. (2005). The Fanconi anemia pathway is required for the DNA replication stress response and for the regulation of common fragile site stability. Hum. Mol. Genet. *14*, 693–701. https://doi.org/10.1093/hmg/ddi065.

28. Chan, K.L., Palmai-Pallag, T., Ying, S., and Hickson, I.D. (2009). Replication stress induces sister-chromatid bridging at fragile site loci in mitosis. Nat. Cell Biol. *11*, 753–760. https://doi.org/10.1038/ncb1882.

29. Minocherhomji, S., Ying, S., Bjerregaard, V.A., Bursomanno, S., Aleliunaite, A., Wu, W., Mankouri, H.W., Shen, H., Liu, Y., and Hickson, I.D. (2015). Replication stress activates DNA repair synthesis in mitosis. Nature *528*, 286–290. https://doi.org/10.1038/nature16139.

30. Ying, S., Minocherhomji, S., Chan, K.L., Palmai-Pallag, T., Chu, W.K., Wass, T., Mankouri, H.W., Liu, Y., and Hickson, I.D. (2013). MUS81 promotes common fragile site expression. Nat. Cell Biol. *15*, 1001–1007. https://doi.org/10.1038/ncb2773.

31. Naim, V., Wilhelm, T., Debatisse, M., and Rosselli, F. (2013). ERCC1 and MUS81-EME1 promote sister chromatid separation by processing late

replication intermediates at common fragile sites during mitosis. Nat. Cell Biol. *15*, 1008–1015. https://doi.org/10.1038/ncb2793.

32. Svendsen, J.M., Smogorzewska, A., Sowa, M.E., O'Connell, B.C., Gygi, S.P., Elledge, S.J., and Harper, J.W. (2009). Mammalian BTBD12/SLX4 assembles a Holliday junction resolvase and is required for DNA repair. Cell *138*, 63–77. https://doi.org/10.1016/j.cell.2009.06.030.

33. Wyatt, H.D.M., Laister, R.C., Martin, S.R., Arrowsmith, C.H., and West, S.C. (2017). The SMX DNA repair tri-nuclease. Mol. Cell *65*, 848–860.e11. https://doi.org/10.1016/j.molcel.2017.01.031.

34. Guervilly, J.H., and Gaillard, P.H. (2018). SLX4: multitasking to maintain genome stability. Crit. Rev. Biochem. Mol. Biol. *53*, 475–514. https://doi.org/10.1080/10409238.2018.1488803.

35. Bhat, A., Andersen, P.L., Qin, Z., and Xiao, W. (2013). Rev3, the catalytic subunit of Polζ, is required for maintaining fragile site stability in human cells. Nucleic Acids Res. *41*, 2328–2339. https://doi.org/10.1093/nar/gks1442.

36. Bergoglio, V., Boyer, A.S., Walsh, E., Naim, V., Legube, G., Lee, M.Y.W.T., Rey, L., Rosselli, F., Cazaux, C., Eckert, K.A., and Hoffmann, J.S. (2013). DNA synthesis by Pol η promotes fragile site stability by preventing under-replicated DNA in mitosis. J. Cell Biol. *201*, 395–408. https://doi.org/10.1083/jcb.201207066.

37. Twayana, S., Bacolla, A., Barreto-Galvez, A., De-Paula, R.B., Drosopoulos, W.C., Kosiyatrakul, S.T., Bouhassira, E.E., Tainer, J.A., Madireddy, A., and Schildkraut, C.L. (2021). Translesion polymerase η both facilitates DNA replication and promotes increased human genetic variation at common fragile sites. Proc. Natl. Acad. Sci. USA *118*, e2106477118. https://doi.org/10.1073/pnas.2106477118.

38. Costantino, L., Sotiriou, S.K., Rantala, J.K., Magin, S., Mladenov, E., Helleday, T., Haber, J.E., Iliakis, G., Kallioniemi, O.P., and Halazonetis, T.D. (2014). Break-induced replication repair of damaged forks induces genomic duplications in human cells. Science *343*, 88–91. https://doi.org/10.1126/science.1243211.

39. Kaushal, S., Wollmuth, C.E., Das, K., Hile, S.E., Regan, S.B., Barnes, R.P., Haouzi, A., Lee, S.M., House, N.C.M., Guyumdzhyan, M., et al. (2019). Sequence and nuclease requirements for breakage and healing of a structure-forming (AT)n sequence within fragile site FRA16D. Cell Rep. *27*, 1151–1164.e5. https://doi.org/10.1016/j.celrep.2019.03.103.

40. Ip, S.C.Y., Rass, U., Blanco, M.G., Flynn, H.R., Skehel, J.M., and West, S.C. (2008). Identification of Holliday junction resolvases from humans and yeast. Nature *456*, 357–361. https://doi.org/10.1038/nature07470.

41. Chan, Y.W., and West, S. (2015). GEN1 promotes Holliday junction resolution by a coordinated nick and counter-nick mechanism. Nucleic Acids Res. *43*, 10882–10892. https://doi.org/10.1093/nar/gkv1207.

42. Rass, U., Compton, S.A., Matos, J., Singleton, M.R., Ip, S.C.Y., Blanco, M.G., Griffith, J.D., and West, S.C. (2010). Mechanism of Holliday junction resolution by the human GEN1 protein. Genes Dev. *24*, 1559–1569. https://doi.org/10.1101/gad.585310.

43. Wyatt, H.D.M., Sarbajna, S., Matos, J., and West, S.C. (2013). Coordinated actions of SLX1-SLX4 and MUS81-EME1 for Holliday junction resolution in human cells. Mol. Cell *52*, 234–247. https://doi.org/10.1016/j.molcel.2013.08.035.

44. Chan, Y.W., and West, S.C. (2014). Spatial control of the GEN1 Holliday junction resolvase ensures genome stability. Nat. Commun. *5*, 4844. https://doi.org/10.1038/ncomms5844.

45. Sirbu, B.M., Couch, F.B., and Cortez, D. (2012). Monitoring the spatiotemporal dynamics of proteins at replication forks and in assembled chromatin using isolation of proteins on nascent DNA. Nat. Protoc. *7*, 594–605. https://doi.org/10.1038/nprot.2012.010.

46. Matos, J., Blanco, M.G., Maslen, S., Skehel, J.M., and West, S.C. (2011). Regulatory control of the resolution of DNA recombination intermediates during meiosis and mitosis. Cell *147*, 158–172. https://doi.org/10.1016/j.cell.2011.08.032.

47. Madireddy, A., Kosiyatrakul, S.T., Boisvert, R.A., Herrera-Moyano, E., García-Rubio, M.L., Gerhardt, J., Vuono, E.A., Owen, N., Yan, Z., Olson, S., et al. (2016). FANCD2 facilitates replication through common fragile sites. Mol. Cell *64*, 388–404. https://doi.org/10.1016/j.molcel.2016.09.017.

48. Bhowmick, R., Minocherhomji, S., and Hickson, I.D. (2016). RAD52 facilitates mitotic DNA synthesis following replication stress. Mol. Cell *64*, 1117–1126. https://doi.org/10.1016/j.molcel.2016.10.037.

49. Epum, E.A., and Haber, J.E. (2022). DNA replication: the recombination connection. Trends Cell Biol. *32*, 45–57. https://doi.org/10.1016/j.tcb.2021.07.005.

50. Chan, K.L., North, P.S., and Hickson, I.D. (2007). BLM is required for faithful chromosome segregation and its localization defines a class of ultrafine anaphase bridges. EMBO J. *26*, 3397–3409. https://doi.org/10.1038/sj.emboj.7601777.

51. Di Marco, S., Hasanova, Z., Kanagaraj, R., Chappidi, N., Altmannova, V., Menon, S., Sedlackova, H., Langhoff, J., Surendranath, K., Hühn, D., et al. (2017). RECQ5 helicase cooperates with MUS81 endonuclease in processing stalled replication forks at common fragile sites during mitosis. Mol. Cell *66*, 658–671.e8. https://doi.org/10.1016/j.molcel.2017.05.006.

52. Harrigan, J.A., Belotserkovskaya, R., Coates, J., Dimitrova, D.S., Polo, S.E., Bradshaw, C.R., Fraser, P., and Jackson, S.P. (2011). Replication stress induces 53BP1-containing OPT domains in G1 cells. J. Cell Biol. *193*, 97–108. https://doi.org/10.1083/jcb.201011083.

53. Spies, J., Lukas, C., Somyajit, K., Rask, M.B., Lukas, J., and Neelsen, K.J. (2019). 53BP1 nuclear bodies enforce replication timing at under-replicated DNA to limit heritable DNA damage. Nat. Cell Biol. *21*, 487–497. https://doi.org/10.1038/s41556-019-0293-6.

54. Chan, Y.W., Fugger, K., and West, S.C. (2018). Unresolved recombination intermediates lead to ultra-fine bridges, chromosome breaks and aberrations. Nat. Cell Biol. *20*, 92–103. https://doi.org/10.1038/s41556-017-0011-1.

55. Rageul, J., Frëmin, C., Ezan, F., Baffet, G., and Langouët, S. (2011). The knock-down of ERCC1 but not of XPF causes multinucleation. DNA Repair *10*, 978–990. https://doi.org/10.1016/j.dnarep.2011.07.005.

56. Hoffelder, D.R., Luo, L., Burke, N.A., Watkins, S.C., Gollin, S.M., and Saunders, W.S. (2004). Resolution of anaphase bridges in cancer cells. Chromosoma *112*, 389–397. https://doi.org/10.1007/s00412-004-0284-6.

57. Tapia, C., Kutzner, H., Mentzel, T., Savic, S., Baumhoer, D., and Glatz, K. (2006). Two mitosis-specific antibodies, MPM-2 and phospho-histone H3 (Ser28), allow rapid and precise determination of mitotic activity. Am. J. Surg. Pathol. *30*, 83–89. https://doi.org/10.1097/01.pas.0000183572.94140.43.

58. Ji, F., Liao, H., Pan, S., Ouyang, L., Jia, F., Fu, Z., Zhang, F., Geng, X., Wang, X., Li, T., et al. (2020). Genome-wide high-resolution mapping of mitotic DNA synthesis sites and common fragile sites by direct sequencing. Cell Res. *30*, 1009–1023. https://doi.org/10.1038/s41422-020-0357-y.

59. Wechsler, T., Newman, S., and West, S.C. (2011). Aberrant chromosome morphology in human cells defective for Holliday junction resolution. Nature *471*, 642–646. https://doi.org/10.1038/nature09790.

60. Sarbajna, S., Davies, D., and West, S.C. (2014). Roles of SLX1-SLX4, MUS81-EME1 and GEN1 in avoiding genome instability and mitotic catastrophe. Genes Dev. *28*, 1124–1136. https://doi.org/10.1101/gad.238303.114.

61. Loupart, M.-L., Krause, S.A., and Heck, M.S. (2000). Aberrant replication timing induces defective chromosome condensation in *Drosophila* ORC2 mutants. Curr. Biol. *10*, 1547–1556. https://doi.org/10.1016/s0960-9822(00)00844-7.

62. Pflumm, M.F., and Botchan, M.R. (2001). *ORC* mutants arrest in metaphase with abnormally condensed chromosomes. Development *128*, 1697–1707. https://doi.org/10.1242/dev.128.9.1697.

63. Reinhold, W.C., Sunshine, M., Liu, H., Varma, S., Kohn, K.W., Morris, J., Doroshow, J., and Pommier, Y. (2012). CellMiner: a web-based suite of genomic and pharmacologic tools to explore transcript and drug patterns in the NCI-60 cell line set. Cancer Res. *72*, 3499–3511. https://doi.org/10.1158/0008-5472.CAN-12-1370.

64. Fuchs, J., Cheblal, A., and Gasser, S.M. (2021). Underappreciated roles of DNA polymerase δ in replication stress survival. Trends Genet. *37*, 476–487. https://doi.org/10.1016/j.tig.2020.12.003.

65. Garner, E., Kim, Y., Lach, F.P., Kottemann, M.C., and Smogorzewska, A. (2013). Human GEN1 and the SLX4-associated nucleases MUS81 and SLX1 are essential for the resolution of replication-induced Holliday junctions. Cell Rep. *5*, 207–215. https://doi.org/10.1016/j.celrep.2013.08.041.

66. Ran, F.A., Hsu, P.D., Wright, J., Agarwala, V., Scott, D.A., and Zhang, F. (2013). Genome engineering using the CRISPR-Cas9 system. Nat. Protoc. *8*, 2281–2308. https://doi.org/10.1038/nprot.2013.143.

67. Young, S.J., Sebald, M., Shah Punatar, R., Larin, M., Masino, L., Rodrigo-Brenni, M.C., Liang, C.C., and West, S.C. (2020). MutSβ stimulates Holliday junction resolution by the SMX complex. Cell Rep. *33*, 108289. https://doi.org/10.1016/j.celrep.2020.108289.

68. Chan, Y.W., and West, S.C. (2018). GEN1 endonuclease: purification and nuclease assays. In Methods in Enzymology, M. Spies and A. Malkova, eds. (Academic Press), pp. 527–542. https://doi.org/10.1016/bs.mie.2017.11.020.

STAR★METHODS

KEY RESOURCES TABLE

REAGENT or RESOURCE	SOURCE	IDENTIFIER
Antibodies		
Rabbit polyclonal anti-GEN1 (CT SCY5)	This laboratory[42]	N/A
Rabbit polyclonal anti-MUS81 (MTA30 2G10/3)	This laboratory[33]	Abcam Cat# ab14387; RRID:AB_301167
Rabbit polyclonal anti-CyclinA2	Abcam	Cat# ab137769
Mouse monoclonal anti-CylinA2 (6B4D11)	Thermo Fisher	Cat# 6B4D11; RRID:AB_2633305
TAT1 mouse anti-α-tubulin	Sigma-Aldrich	Cat# 00020911; RRID:AB_10013740
Rabbit polyclonal anti-Histone H3	Abcam	Cat# ab1791; RRID:AB_302613
Rabbit polyclonal anti-FANCD2	Novus Biologicals	Cat# NB100-182; RRID:AB_10002867
Mouse monoclonal anti-FANCD2 (FI17)	Santa Cruz	Cat# Sc-20022; RRID:AB_2278211
Rabbit polyclonal anti-Lamin B1	Abcam	Cat# ab16048; RRID:AB_443298
Mouse monoclonal anti- RPA32/RPA2 (9H8)	Abcam	Cat# ab2175; RRID:AB_302873
Rabbit polyclonal anti-RPA32/RPA2	Abcam	Cat# ab10359; RRID:AB_297095
Mouse monoclonal anti-PICH (142-26-3)	Sigma-Aldrich	Cat# 04–1540; RRID:AB_11210090
Rabbit polyclonal anti-53BP1	Abcam	Cat# ab36823; RRID:AB_722497
Rabbit polyclonal anti-53BP1	Novus Biologicals	Cat# NB100-304; RRID:AB_10003037
Rabbit polyclonal anti-γ-H2AX (S139)	Abcam	Cat# ab2893; RRID:AB_303388
Mouse monoclonal anti-PCNA (PC10)	Abcam	Cat# ab29; RRID:AB_303394
Rabbit monoclonal anti-POLD1 (EPR15118)	Abcam	Cat# ab186407; RRID:AB_2921290
Rabbit monoclonal anti-POLD3 (EP9480)	Abcam	Cat# ab182564
Rat monoclonal anti-BrdU (BU1/75 (ICR1))	Thermo Fisher	Cat# MA1-82088; RRID:AB_927214
Mouse monoclonal anti-BrdU (B44)	BD Biosciences	Cat# 347580; RRID:AB_10015219
Goat polyclonal anti-mouse HRP	Agilent	Cat# P0447; RRID:AB_2617137
Goat polyclonal anti-rabbit HRP	Agilent	Cat# P0448; RRID:AB_2617138
Mouse monoclonal anti-phospho-Ser/Thr-Pro MPM-2 antibody, Cy5 conjugate	Sigma-Aldrich	Cat# 16–220; RRID:AB_442398
Goat anti-mouse IgG (H + L) cross-adsorbed secondary antibody, Alexa Fluor 488	Thermo Fisher	Cat# A-11001; RRID:AB_2534069
Goat anti-rabbit IgG (H + L) cross-adsorbed secondary antibody, Alexa Fluor 488	Thermo Fisher	Cat#A-11008; RRID:AB_143165
Goat anti-mouse IgG (H + L) highly cross-adsorbed secondary antibody, Alexa Fluor 555	Thermo Fisher	Cat# A-21424; RRID:AB_141780
Donkey anti-rabbit IgG (H + L) highly Cross-Adsorbed Secondary Antibody, Alexa Fluor 555	Thermo Fisher	Cat# A-31572; RRID:AB_162543
Goat anti-Rat IgG (H + L) cross-adsorbed secondary antibody, Alexa Fluor 568	Thermo Fisher	Cat# A-11077; RRID. AB_2534121
Chemicals, peptides, and recombinant proteins		
Aphidicolin	Sigma-Aldrich	Cat# A4487
DMSO	Sigma-Aldrich	Cat# D2650
Benzonase nuclease	Sigma-Aldrich	Cat# E1014
DPX mountant	Sigma-Aldrich	Cat# 06522
Giemsa	Sigma-Aldrich	Cat# 48900
ProLong Gold antifade mountant with DAPI reagent	Thermo Fisher	Cat# P36931
ProLong Gold antifade mountant	Thermo Fisher	Cat# P36934
SYTOX Green	Thermo Fisher	Cat# S7020

(Continued on next page)

Continued

REAGENT or RESOURCE	SOURCE	IDENTIFIER
Halt protease and phosphatase inhibitor cocktail (100X)	Thermo Fisher	Cat# 78446
Lipofectamine RNAiMAX	Thermo Fisher	Cat# 13778100
Lipofectamine 2000	Thermo Fisher	Cat# 11668030
GenJet *in vitro* DNA transfection reagent	SignaGen Laboratories	Cat# SL100488
Polybrene	Sigma	Cat# TR-1003-G
FuGENE HD transfection reagent	Promega	Cat# E2311
baculoQUAN ALL-IN-ONE virus extraction & titration kit	Oxford Expression Technologies	Cat# 100602
Sf-900 III SFM	Thermo Fisher	Cat# 12658019
Opti-MEM I reduced serum medium	Thermo Fisher	Cat# 31985070
Dulbecco's modified Eagle's medium (DMEM)	Thermo Fisher	Cat# 41966029
Iscove's modified Dulbecco's medium (IMDM)	Thermo Fisher	Cat# 21980065
Tetracycline-free FBS	PAN Biotech	Cat# P30-3602
FBS	Sigma-Aldrich	Cat# F7524
Penicillin-streptomycin	Sigma-Aldrich	Cat# P4333
Propidium iodide	Sigma-Aldrich	Cat# P4864
ON-TARGETplus non-targeting control siRNA #1	Dharmacon	Cat# D-001810-01-05
ON-TARGETplus GEN1 siRNA (5′-GUAAAGACCUGC AAUGUUAUU-3′)	Dharmacon	Cat# CTM-265563
ON-TARGETplus Human MUS81 siRNA	Dharmacon	Cat# J-016143-09 and J-016143-10
ON-TARGETplus Human POLD1 siRNA	Dharmacon	Cat# L-019687-00-0005
ON-TARGETplus Human POLD3 siRNA	Dharmacon	Cat# L-026692-01-0005
Colcemid	Sigma-Aldrich	Cat# 10295892001
iQ SYBR Green Supermix reagent	Bio Rad	Cat# 1708880
Ribonuclease A	Qiagen	Cat# 151032014
Pierce 16% Formaldehyde (w/v), Methanol-free	Thermo Fisher	Cat# 28908
CellTiter-Glo Luminescent Cell Viability Assay	Promega	Cat# G7572
RNase A	Qiagen	Cat# 19101
Biotin azide	Invitrogen	Cat# B10184
Ni-NTA agarose	Qiagen	Cat# 30210
Resource Q column	Cytiva	Cat# 17117701
Superdex 200 Increase 10/300 column	Cytiva	Cat# 28990945
Corning BioCoat 12mm #1 german glass coverslips, round	Thermo Fisher	Cat# 08-774-384
Click-iT Plus EdU Alexa Fluor 488 flow cytometry assay kit	Thermo Fisher	Cat# C10632
Click-iT Plus EdU Alexa Fluor 647 flow cytometry assay kit	Thermo Fisher	Cat# C10634
QIAamp DNA mini kit	Qiagen	Cat# 51304
Invitrogen GeneArt gene synthesis	Thermo Fisher	N/A
TaqMan Copy Number Assay, WWOX, Hs07550079_cn	Thermo Fisher	Cat# 4400291
TaqMan Copy Number Assay, NGR3, Hs05145206_cn	Thermo Fisher	Cat# 4400291
Experimental models: Cell lines		
Flp-In-T-Rex-293	The Francis Crick Institute Cell Services	N/A
U2OS	The Francis Crick Institute Cell Services	N/A
HK-2	The Francis Crick Institute Cell Services	N/A
293FT	The Francis Crick Institute Cell Services	N/A

Continued

REAGENT or RESOURCE	SOURCE	IDENTIFIER
Oligonucleotides		
GEN1 3rd exon guide 1 5′-CACCGATGGGTCTTCTGGAAAATCG-3′	Thermo Fisher	N/A
GEN1 3rd exon guide 2 5′-CACCGAAGCTGATGTCATAAGCAAG-3′	Thermo Fisher	N/A
MUS81 3rd exon 5′-CACCGAGAGCACCAGCAGTATCACT-3′	Thermo Fisher	N/A
MUS81 4th exon 5′-CACCGAGAACAGTCCAGCCCCGCAG-3′	Thermo Fisher	N/A
Oligo 1 5′-ACGCTGCCGAATTCTACCAGTG CCTTGCTAGGAC ATCTTTGCCCACCTGCAGGTTCACCC-3′	Sigma-Aldrich[33]	Custom
Oligo 4 5′-CGATAGTCGGATCCTCTAGACAGCT CCATGTAGC AAGGCACTGGTAGAATTCGGCAGCGT-3′	Sigma-Aldrich[33]	Custom
Oligo 2.5 5′-GGGTGAACCTGCAGGTGGGCAA AGATGTCC-3′	Sigma-Aldrich[33]	Custom
Oligo 3.5 5′-CATGGAGCTGTCTAGAGGATC CGACTATCG-3′	Sigma-Aldrich[33]	Custom
Recombinant DNA		
hSpCas9 lentiCRISPRv2	Addgene	Plasmid ID 52961
lenti-sgRNA-Puro	Addgene	Plasmid ID 52963
lenti-sgRNA-Hygro	Addgene	Plasmid ID 104991
ViraPower Packaging Mix: pLP1, pLP2, pLP/VSVG	Thermo Frisher	Cat# K4975-00
pBIG1a	Addgene	Plasmid ID 80611
pSpCas9(BB)	Addgene	Plasmid ID 42230
Software and algorithms		
Prism	GraphPad	https://www.graphpad.com/scientific-software/prism/
Volocity	Volocity	https://www.volocity4d.com/download
IDEAS (Image Data Exploration and Analysis Software)	Luminex	https://www.luminexcorp.com/eu/imaging-flow-cytometry/
DEVA	Roche	https://eagle.fish.washington.edu/bivalvia/array/nimblegen/User_Guides/Application_Guides/NG_CGX_UGuide_v3p1.pdf
FACSDiva	BD Biosciences	https://www.bdbiosciences.com/en-gb/products/software/instrument-software/bd-facsdiva-software
FlowJo	FlowJo	https://www.flowjo.com/
GelCount	Oxford Optronics	https://www.oxford-optronix.com/gelcount
Cellomics spot detector bioapplication	Thermo Fisher	N/A

RESOURCE AVAILABILITY

Lead contact
Further information and requests for resources and reagents should be directed to and will be fulfilled by the Lead Contact, Stephen C. West (stephen.west@crick.ac.uk).

Materials availability
Materials and cell lines generated in this study are available from the Lead Author with no restrictions.

Data and code availability

- The raw data for the manuscript is available on request from the lead contact Dr. Stephen C. West (stephen.west@crick.ac.uk).
- The paper does not report new or original code.
- Any additional information required to reanalyze the data reported in this paper is available from the lead author on request.

EXPERIMENTAL MODEL AND SUBJECT DETAILS

Cell lines

Flp-In™ T-REx-293 cells (HEK293) were grown in Dulbecco's modified Eagle's medium (DMEM) supplemented with 10% tetracycline-free FBS. 293FT and U2OS cells were grown in DMEM supplemented with 10% FBS. All cultures were grown in 1x penicillin-streptomycin and maintained at 37°C and 5% CO_2. Cell line authentication was performed by STR profiling in the Cell Services science technology platform at The Francis Crick Institute.

METHOD DETAILS

Pool lentiviral CRISPR knockout

Guide RNA targets were designed using Benchling's CRISPR guide RNA design tool against the third exon of *GEN1* (ENSG00000178295) and the third and fourth exons of *MUS81* (ENSG00000172732). Guides were cloned into the lentiGuide-hygro and lentiCRISPRv2 vector system, which encodes for hSpCas9 and a gene-specific chimeric guide RNA. 293FT cells (5×10^6) were seeded in T75 flasks and allowed to recover for 24 h prior to transfection with lentiviral packaging plasmids pLP1 (2.8 μg), pLP2 (1.3 μg), pLP/VSVG (1.9 μg), the expression plasmids lentiCRISPRv2 or lentiGuide-hygro (5 μg), and Lipofectamine 2000 transfection reagent in serum and antibiotic free medium. Next day, the medium was replaced with DMEM supplemented with 10% FBS and cells were allowed to produce virus for the following 48 h. Virus particles were filtered and used immediately or frozen at −80°C for long-term storage. Pool *GEN1* k/o and *MUS81* k/o cells were generated through lentiviral transduction of suspended HEK293 cells with guide RNA virus in complete medium supplemented with 8 μg/mL polybrene. Next day, the cells were selected with 0.67 μg/mL puromycin for 7 days and knockout efficiency was assessed by Western blot. To generate double k/o's, HEK293 cells were transduced with lentiGuide-hygro vectors carrying sgRNA for one gene, followed by selection with 200 μg/mL hygromycin for 7 days, and a second transduction with the lentiCRISPRv2 carrying hSpCas9 and sgRNA for the other gene. All target guides and combinations were assessed by western blotting.

Single cell CRISPR knockout

U2OS *GEN1* k/o cells were derived using the CRISPR-Cas9 system as described[66] by targeting the second exon (5′-CACATCCCCTTGCGTAATCT-3′) with pSpCas9(BB) plasmid containing both Cas9 and the sgRNA scaffold. 6×10^5 cells were seeded and transfected the following day with 1 μg pSpCas9(BB) and GenJet transfection reagent. Next day, single cells were sorted by flow cytometry and allowed to form colonies. Clones were validated by CloneJET PCR blunt-end cloning and DNA sequencing revealing a 10 base pair deletion (CCCCTTG———————GTGGG) in *GEN1*. Further validation was performed by immunoblotting.

siRNA interference

Cells were seeded and allowed to recover for 24 h prior to transfection with 40 nM ON-TARGETplus Non-targeting Control siRNA, or ON-TARGETplus siGEN1, MUS81, POLD1, or POLD3 siRNA and Lipofectamine RNAiMAX transfection reagent in serum and antibiotic-free medium. The medium was supplemented with 10% FBS 8 h post-transfection. Cells were allowed to recover for 48 h for optimal knockdown prior to further experimental procedures.

Metaphase chromosome spreads

Cells were treated with APH (0.2–0.4 μM), or DMSO (control), for 24 h followed by release and treatment with 0.2 μg/mL colcemid for 1 h at 37°C. They were harvested, resuspended drop-wise in pre-warmed hypotonic solution (75 mM KCl) and incubated for 10 min at 37°C. Pelleted cells were fixed by addition of fresh 3:1 methanol:acetic acid drop-wise and incubation for 15 min at room temperature (RT). Fixation was repeated three times. The cells were spread onto slides and aged for 24 h before staining with 7% Giemsa and 10 mM PIPES solution for 10 min at RT. Slides were dried overnight and mounted with DPX mountant solution. Metaphase chromosomes were visualized using a 100X oil immersion objective and bright field channel on an upright Zeiss fluorescence microscope AxioImager. Images were acquired using Volocity software. Quantifications of breaks and constrictions were done manually.

Immunofluorescence on chromosome spreads

Chromosome spreads were prepared as above with the following exceptions. To detect mitotic DNA synthesis (MiDAS), cells were incubated with 20 μM 5-ethynyl-2′-deoxyuridine (EdU) and 0.2 μg/mL colcemid for 30 min prior to tripsinization. Following one round of fresh 3:1 methanol:acedic acid fixation, the cells were dropped onto slides, allowed to dry briefly, and immediately submerged in

PBS for 5 min. EdU was detected through Click-iT reaction and Alexa Fluor® 647 azide as recommended by the manufacturer (Thermo Fisher) for 1 h at RT. The reaction was quenched with 3% BSA in PBS for 5 min and chromosome staining was performed with SYTOX-green (0.6 nM) for 10 min at RT. Slides were mounted with ProLong™ Gold Antifade Mountant. Metaphase chromosomes were visualized using a 100X oil immersion objective on an upright Zeiss fluorescence microscope AxioImager. Images were acquired using Volocity software. Quantifications of EdU on breaks and constrictions were done manually.

Immunofluorescence

Cells were seeded onto 12 mm Poly-D-Lysine coated slides and treated with APH or DMSO (control) for 24 h, followed by fixation in 20 mM PIPES, 0.2% Triton X-100, 10 mM EGTA, 1 mM MgCl$_2$, and 4% formaldehyde for 10 min at RT. For MiDAS experiments, cells were released from APH treatment into pre-equilibrated warmed medium containing 20 µM EdU and 0.2 µg/mL colcemid for 30 min followed by fixation. Cells were permeabilized in 0.5% Triton X-100 in PBS for 10 min at RT. Immunodetection consisted of blocking for 1 h at RT with 3% BSA in PBS, primary antibody incubation in 3% BSA in PBS overnight at 4°C, and secondary incubation in 3% BSA in PBS for 2 h at RT. The antibodies used were: FANCD2 rabbit polyclonal (1:1000, Novus), PICH mouse monoclonal (1:150, Sigma-Aldrich), RPA mouse monoclonal (1:200, Abcam), 53BP1 rabbit polyclonal (1:500, Abcam), CyclinA mouse monoclonal (1:200, Thermo Fisher) and secondary antibodies conjugated to Alexa Fluor 488 or 555 (1:1000, Thermo Fisher). Negative staining of Cyclin A was used to identify cells in G1 phase. EdU detection was performed as described above following protein detection. Slides were mounted with ProLong™ Gold Antifade Mountant with DAPI reagent. Images were acquired using an upright Zeiss fluorescence microscope AxioImager equipped with a 40X, 63X, and 100X oil immersion objective and Volocity software. High throughput screening was performed using the Cellomics ArrayScan VTI 65.2 using 20X (NA0.4) objective. Images were analyzed using the SpotDetector Bioapplication (details available on request).

Flow cytometry

Cells were treated with APH (0.2 or 0.4 µM), or DMSO, for 24 h, and then trypsinized and fixed drop-wise in 70% ethanol for 1 h at 4°C. To label DNA, cells were supplemented with 50 µg/mL propidium iodide, 0.1 mg/mL RNase A, and labeled for 60 min at RT. Flow cytometry and data collection was performed using the LSRFortessa™ and FACSDIVA™ acquisition software. Cells were imaged using a 610/20 yellow bandpass filter and 561 nm excitation laser. Data analysis was performed using FlowJo software version 10. Cell doublets were excluded from the final analysis. Cell cycle analysis was performed using the Watson (Pragmatic) model.

Subcellular fractionation

Cells were treated with APH (0.4 µM) or DMSO (control) for 24 h, harvested, and incubated in hypotonic buffer (10 mM Tris-HCl pH 7.5, 10 mM KCl, 1.5 mM MgCl$_2$, 1x protease and phosphatase inhibitor cocktail) for 10 min on ice and lysed by 5 strokes with the tight pestle of a Dounce homogenizer. Nuclei were pelleted by centrifugation at 1,500 x g for 5 min at 4°C, separated from the cytoplasmic fraction (supernatant), and washed 2 times with hypotonic buffer. The nuclear soluble fraction was extracted by resuspension in 0.5 pellet volume of low salt buffer (20 mM Tris-HCl pH 7.5, 20 mM KCl, 1.5 mM MgCl$_2$, 0.2 mM EDTA, 25% glycerol, and 1x protease and phosphatase inhibitor cocktail) and slowly adding 4.5 pellet volume of high salt buffer (20 mM Tris-HCl pH 7.5, 2 M KCl, 1.5 mM MgCl$_2$, 0.2 mM EDTA, 25% glycerol, and 1x protease and phosphatase inhibitor cocktail). The extract was incubated on ice for 15 min and centrifuged at high speed (20,800 x g) for 30 min at 4°C to separate the nuclear soluble (supernatant) fraction from the chromatin/insoluble fraction. The chromatin fraction was washed 2x with high salt buffer, treated with benzonase (25 units/100 µl) for 15 min at RT, and sonicated at high intensity for 8 cycles (30 s on/30 s off) in a Bioruptor ultrasonicator. The chromatin fraction was cleared from the insoluble fraction by centrifugation at high speed (20,800 x g) for 10 min at 4°C.

Isolation of proteins on nascent DNA (iPOND)

iPOND assays were performed essentially as described.[45] HEK293 cells were treated with APH (0.4 µM) or DMSO for 18 h and pulse labeled with EdU (10 µM) for the last 10 min at 37°C and 5% CO$_2$. For the chase samples, cells were washed and incubated with pre-equilibrated medium containing thymidine (10 µM) for 30–90 min at 37°C and 5% CO$_2$ prior to EdU labeling. Protein elution from Streptavidin-agarose beads was performed in 2x NuPAGE™ LDS Sample Buffer for 25 min at 95°C. Proteins were analyzed by SDS-PAGE on a 4–12% Bis-Tris gel and transferred to a PVDF or nitrocellulose membrane for immunoblotting.

Western blotting

Whole cell lysates were prepared in 20 mM Tris-HCl pH 7.5, 150 mM NaCl, 1 mM EDTA, 1% Triton X-100, 10% glycerol, 1x protease and phosphatase inhibitor cocktail (Roche) and 1 mM DTT. The lysates were treated with benzonase for 15 min at RT and sonicated for 8 cycles (30 s on/30 s off) in a Bioruptor ultrasonicator. Lysates were cleared from the insoluble fraction by high speed centrifugation (20,800 x g) for 15 min at 4°C. Samples (30–50 µg) were analyzed by SDS-PAGE and transferred to a PVDF or nitrocellulose membrane for immunoblotting. The antibodies used were: anti-FANCD2 (1:1000, Novus), anti-GEN (1:100, CT SCY5), anti-MUS81 (1:1000, MTA30, Abcam 2G10/3), anti-α-tubulin (1:8000, Sigma-Aldrich), anti-Histone H3 (1:3000, Abcam), anti-PCNA (PC10) (1:2000, Abcam), and anti-Lamin B1 (1:4000, Abcam).

Expression and purification of proteins

Human *RFA1* (RPA1), *RFA2* (RPA2) and *RFA3* (RPA3) with a 10x histidine tag at the N-terminus were synthesised and cloned into a pFastBac1 vector by GeneArt Gene Synthesis. Two copies of RPA1, one copy of RPA2 and one copy of 10xHis-RPA3 were assembled into biGBac expression system pBIG1a vector. The resulting pBIG1a-His-tRPA bacmids were transfected into Sf9 cells with FuGENE HD, and the titer of baculovirus was determined with baculoQUANT. Sf9 cells (500 mL) were grown in Sf-900 III SFM in a 28°C shaking incubator at 140 rpm and infected with pBIG1a-His-tRPA P2 baculovirus at 2 million cells/mL (MOI = 1) and harvested 60–66 h later. The cell pellet was resuspended in lysis buffer (25 mM HEPES pH 8.0, 500 mM NaCl, 10% glycerol, 20 mM imidazole, 0.25 mM TCEP) and supplemented with Halt Protease inhibitors and sonicated to lyse the cells. The lysate was clarified by centrifugation at 49,000 g for 25 min at 4°C. Pre-equilibrated Ni-NTA agarose beads (1 mL) was added to the supernatant and incubated on a rotator at 4°C for 1–2 h. The beads were first washed with 5 column volumes (CV) of lysis buffer, and further washed with 5 CV of lysis buffer containing decreasing NaCl concentration (400, 300, 200 mM, respectively). The recombinant RPA was eluted with 4 mL elution buffer (lysis buffer supplemented with 250 mM imidazole). The recombinant RPA was diluted 2.5 times with buffer containing 25 mM HEPES pH 8.0, 100 mM NaCl, 10% glycerol, 0.25 mM TCEP and Halt Protease inhibitors, and loaded onto a pre-equilibrated 6 mL Resource Q column connected to a AKTA Pure (Cytiva) at 4°C. The recombinant RPA was eluted with linear gradient of buffer containing 25 mM HEPES pH 8.0, 100–600 mM NaCl, 10% glycerol and 0.25 mM TCEP. Peak fractions containing trimeric RPA were pooled, concentrated with Centriprep (30 kDa cutoff) and loaded on a Superdex 200 Increase 10/300 column. The recombinant RPA was eluted with buffer containing 25 mM HEPES pH 8.0, 200 mM KOAc, 0.5 mM EDTA, 10% glycerol and 0.25 mM TCEP. The peak fractions containing pure trimeric RPA were pooled, aliquoted, snap frozen in liquid nitrogen and stored at −80°C.

GEN1, MUS81-EME1 and SLX1-SLX4-MUS81-EME1-XPF-ERCC1 (SMX) were expressed and purified as described.[67,68]

DNA cleavage reactions

Gel-purified oligonucleotide X0-1 was 5′-^{32}P-end-labeled with [γ-^{32}P]-ATP for 1 h at 37°C with T4 polynucleotide kinase. Unincorporated ^{32}P isotopes were removed using a MicroSpin^{TM} G-25 column. The 5′-flap structure was prepared by annealing oligo X0-1 with X0-4 and X0-2.5. The 3′-flap structure comprised oligo X0-1 with X0-4 and X0-3.5. Annealing and purification was carried out essentially as described.[68] Cleavage reactions were carried out in 50 mM Tris-HCl pH 8.4, 1 mM MgCl$_2$, 0.1 mg/mL BSA and 1 mM dithiothreitol for 30 min at 37°C. DNA was pre-incubated with RPA for 10 min at 37°C, the reaction was then supplemented with nuclease and incubated for a further 30 min at 37°C. Reactions were stopped with 2 mg/mL proteinase K and 0.5% (w/v) SDS for 10 min at 37°C, and cleavage products were analyzed by 10% neutral PAGE (150 V for 1 h at RT). Labeled DNA was visualized by autoradiography and quantified.

Electrophoretic mobility shift assay (EMSA)

The binding of purified RPA to 5′-^{32}P-end-labeled 5′-flap and 3′-flap substrates was performed in 50 mM Tris-HCl pH 8.4, 1 mM MgCl$_2$, 0.1 mg/mL BSA and 1 mM DTT for 10 min at 37°C. Samples were placed on ice and loading dye was added (6x: 50% glycerol, 0.1% bromophenol blue, 0.1% xylene cyanol). Products were separated on a 10% native PAGE gel in 1x TBE buffer at 4°C at 150 V for 1 h and visualized by autoradiography.

Imagestream analysis of micronucleation and multinucleation

Cells were treated with APH (0.4 μM) or DMSO (control) for 24hr, trypsinized, and fixed in 70% ethanol for 1 h at 4°C. Blocking was done by washing once with FBS in PBS (2% v/v). Antibody incubation was carried out in 100 μL of CY5-conjugated anti-MPM2 (1:200 in PBS, 0.1% BSA, 0.2% Tween 20) for 1 h at RT in the dark. Following antibody staining, cells were washed twice with FBS in PBS (2% v/v), resuspended at 2 × 10^7 cells/mL in FBS in PBS (2% v/v), and supplemented with 1 μg/mL propidium iodide and 100 μg/mL ribonuclease A. DNA labeling was carried out for 15 min at RT. Flow cytometry and data collection was performed using an ImageStream®^{X} Mark II Imaging Flow Cytometer and INSPIRE® acquisition software. Images were acquired using the bright field channel 1 and fluorescent channel 5 (Bands 640–745 nm) with excitation laser 561 at 150-200mW. Image analysis was performed using IDEAS® software version 6.2. Single cells were filtered using a scatterplot of bright field aspect ratio and cell area. The propidium iodide signal was inspected using the intensity channel 5 M05. In-focus cells were filtered using a root-mean-square histogram with Gradient RMS >50 within the bright field parameter. Non-mitotic cells were selected from a scatterplot of PI intensity versus MPM2 intensity. Cells were inspected manually for micronucleus and multinucleus formation.

Cell viability and survival

Growth curve analysis was performed by seeding the same number of cells and analyzing for viability on an EnSight Multimode Plate Reader at the indicated time points using CellTiter-Glo viability reagent. Cell survival analyses were performed by seeding the same number of HEK293 WT, *GEN1* k/o and *MUS81* k/o cells in the presence of increasing aphidicolin or DMSO for 120hr.

Copy number variation (CNV)

Cells were treated with APH (0.2 μM) or DMSO (control) for 48 h, released for 24 h, and re-seeded into single cells for clonal expansion. Once clones reached confluency in 6 cm dishes, k/o efficiency was confirmed by western blotting. Genomic DNA was isolated from tripsinized cell cultures, pelleted and vortexed in lysis buffer (20 mM Tris-HCl pH 8.0, 85 mM KCl, 0.5% NP-40) for 30 s. Nuclei

were pelleted at 3,300 x g for 5 min at 4°C, resuspended in TE pH 8.0, 1% SDS, 100 μg/mL RNase A, and incubated at RT for 30 min. Proteinase K (200 μg/mL) digestion was performed overnight at RT, followed by phenol:chloroform:isoamyl alcohol extraction. CNV analysis was performed from genomic DNA using real-time PCR and site-specific TaqMan assays. Quantitative real-time PCR reactions were carried out in triplicate as specified by the manufacturer (Thermo Fisher) using 20 ng genomic DNA per sample. RNase P was used as a reference assay for all reactions.

QUANTIFICATION AND STATISTICAL ANALYSIS

Statistical analysis

PRISM unpaired two-tailed t test and EXCEL or PRISM one-way ANOVA data analysis tools were used to calculate statistical significance. Significance was defined as *$p \leq 0.05$, **$p \leq 0.01$, ***$p \leq 0.001$, ****$p \leq 0.0001$.